AGU PUBLICATIONS

Geophysical Research Letters

RESEARCH LETTER
10.1002/2016GL068424

Key Points:
- Mid-mantle seismic and gravity anomaly under Greenland identified
- Jurassic-Cretaceous slab linked to paleo-Arctic ocean closure, prior to Amerasia Basin opening
- Possible arc-mantle signature in Cretaceous High Arctic LIP volcanism

Supporting Information:
- Supporting Information S1

Correspondence to:
G. E. Shephard,
g.e.shephard@geo.uio.no

Citation:
Shephard, G. E., R. G. Trønnes, W. Spakman, I. Panet, and C. Gaina (2016), Evidence for slab material under Greenland and links to Cretaceous High Arctic magmatism, *Geophys. Res. Lett.*, *43*, 3717–3726, doi:10.1002/2016GL068424.

Received 13 OCT 2015
Accepted 18 APR 2016
Accepted article online 19 APR 2016
Published online 27 APR 2016

Evidence for slab material under Greenland and links to Cretaceous High Arctic magmatism

G. E. Shephard[1], R. G. Trønnes[1,2], W. Spakman[1,3], I. Panet[4], and C. Gaina[1]

[1]Centre for Earth Evolution and Dynamics (CEED), Department of Geosciences, University of Oslo, Oslo, Norway, [2]Natural History Museum, University of Oslo, Oslo, Norway, [3]Department of Earth Sciences, Utrecht University, Utrecht, Netherlands, [4]Institut National de l'Information Géographique et Forestière, Laboratoire LAREG, Université Paris Diderot, Paris, France

Abstract Understanding the evolution of extinct ocean basins through time and space demands the integration of surface kinematics and mantle dynamics. We explore the existence, origin, and implications of a proposed oceanic slab burial ground under Greenland through a comparison of seismic tomography, slab sinking rates, regional plate reconstructions, and satellite-derived gravity gradients. Our preferred interpretation stipulates that anomalous, fast seismic velocities at 1000–1600 km depth imaged in independent global tomographic models, coupled with gravity gradient perturbations, represent paleo-Arctic oceanic slabs that subducted in the Mesozoic. We suggest a novel connection between slab-related arc mantle and geochemical signatures in some of the tholeiitic and mildly alkaline magmas of the Cretaceous High Arctic Large Igneous Province in the Sverdrup Basin. However, continental crustal contributions are noted in these evolved basaltic rocks. The integration of independent, yet complementary, data sets provides insight into present-day mantle structure, magmatic events, and relict oceans.

1. Introduction

The tectonic evolution of ocean basins can be deciphered from morphological and geophysical signatures preserved by oceanic crust and adjacent margins, including ophiolites, suture zones, and arc magmatism. Several decades of global data collection including magnetic and gravity anomalies provide key constraints for plate tectonic reconstructions and have been summarized and embedded in recent global models covering hundreds of millions of years [*Seton et al.*, 2012; *Domeier and Torsvik*, 2014]. However, in remote and complex regional tectonic settings dominated by several cycles of ocean basin opening and closure, such data are often spatially and temporally restricted and offer limited information about the geometry and timing of subducted oceanic lithosphere. Deciphering the tectonic evolution of continents and adjacent oceans in frontier regions such as the Arctic remains a challenge.

A large portion of the present Arctic Ocean is occupied by the Amerasia Basin (Figure 1), of which there is significant debate about the nature of its crust and timing of formation. Opening of the Amerasia Basin sometime during the Late Jurassic-Early Cretaceous [e.g., *Grantz et al.*, 2011; *Alvey et al.*, 2008] is considered to have been at the expense of subducting adjacent oceanic lithosphere (~1000 km wide) [e.g., *Nokleberg et al.*, 2000; *Sokolov et al.*, 2002; *Shephard et al.*, 2013]. In most regional reconstructions, the Amerasia Basin is formed by the rotation of Chukotka and the North Slope of Alaska (NSA; also referred to as the "Alaska-Chukotka microplate") away from the Canadian Arctic Islands (e.g., *Lawver et al.* [2002]; see review in *Shephard et al.* [2013]) though other mechanisms have been suggested [e.g., *Miller et al.*, 2010]. Geological evidence for a prior oceanic basin adjacent to northernmost Panthalassa includes the South Anuyi and Angayucham sutures (Figure 1), which run approximately from the New Siberian Islands to Alaska and are delineated by turbidites, ophiolites, granodiorites, and arc volcanic rocks [e.g., *Rowley and Lottes*, 1988; *Drachev et al.*, 1998].

An extinct Arctic Paleozoic-Mesozoic ocean, broadly located between the reconstructed NSA, Chukotka, and Kolyma/Siberia blocks, is often referred to as the South Anuyi-Angayucham Ocean (Figure 2). Regional subduction events during the Middle Jurassic-Early Cretaceous, include the Koyukuk, Oloy, and Nutesyn arcs, related to subduction and collision along the NSA, Kolyma-Omolon terrane, and Chukotka, respectively (Figure 2 and Figure S12 in the supporting information). The timing of final ocean closure along the suture (in at least the western regions) is given by a range of Early Cretaceous (pre-Albian) syncollisional and postcollisional dates including cross-cutting plutons (post-tectonic ~117 Ma) [*Miller et al.*, 2009; *Amato et al.*, 2015],

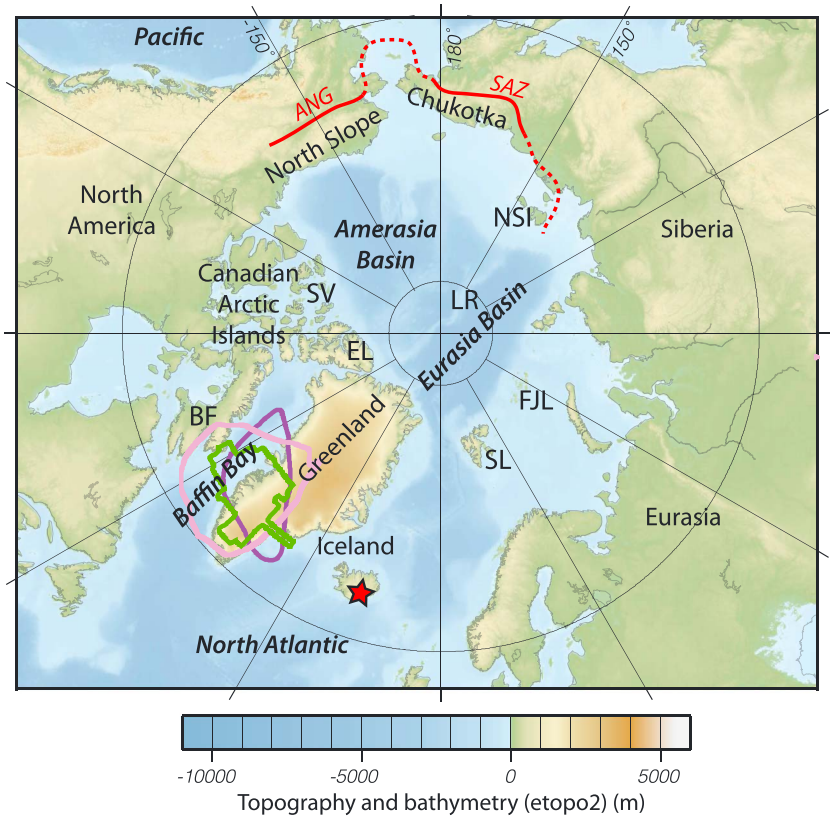

Figure 1. Overview of present Arctic Ocean region. BF: Baffin Island, EL: Ellesmere Island, FJL: Franz Josef Land, LR: Lomonosov Ridge, NSI: New Siberian Islands, SL: Svalbard, SV: Sverdrup Basin. Red line shows location of the Angayucham (ANG) and South Anuyi (SAZ) sutures, which are often linked, as indicated by the stippled lines [*Miller et al*., 2006]; red star: present-day Iceland hotspot. Purple/green lines are approximate Greenland slab extent around 1450 km (0.3% contour; dark purple: *S40RTS* [*Ritsema et al*., 2011], light purple: *GyPSuMS* [*Simmons et al*., 2010]; 0.15% contour, green: *UU-P07* [*Amaru*, 2007], Figure 3).

syncollisional sandstones (125 Ma maximum depositional age; *Amato et al*. [2015]; see also *Moore et al*. [2015] for summary of Brooks Range) and metamorphic domes (124–117 Ma) [*Toro et al*., 2003].

It is worth noting that alternative reconstructions to this singular ocean exist, whereby the NSA and Chukotka terranes are separate prior to Aptian (~125–113 Ma) times. These models reserve "South Anuyi" to the Chukotka-Kolyma/Siberia region and "Angayucham" to the NSA-adjacent area (Figure 2a) [*Amato et al*., 2015; *Till*, 2016]. This implies that the South Anuyi-Angayucham suture, while appearing linked at present day, is in fact two (or more) separate sutures. Regardless of one or more oceanic domains, Late Jurassic-Cretaceous subduction along the NSA (and often Chukotka), associated with its counterclockwise rotation and opening of the Amerasia Basin, is depicted in most tectonic models to date and represents the final stage of South Anuyi-Angayucham closure (Figure 2).

Ambiguity in published reconstructions and the generation of kinematically consistent and linked plate boundaries make a more detailed regional analysis beyond the scope of this study. Indeed, other ophiolite outcrops and sutures related to discrete episodes could be considered in reconstructing the South Anuyi-Angayucham history (e.g., Koyukuk arc and Kolyuchin-Mechigmen zone [*Till*, 2016]). Here we suggest that either Middle Jurassic-Cretaceous tectonic scenario, i.e., discrete spatial and/or temporal subduction episodes (approximately within 10–20 Myr, 500–1000 km), or a single ocean might account for the mantle slab structures discussed below. Notably, the size and robustness of the seismic anomaly under Greenland points to an ocean that was inboard from the main plates of Panthalassa and was likely separated by a long-lived offshore arc system [*Sigloch and Mihalynuk*, 2013; *Miller et al*., 2013]. For clarity we herein refer to this general area as the South Anuyi-Angayucham Ocean.

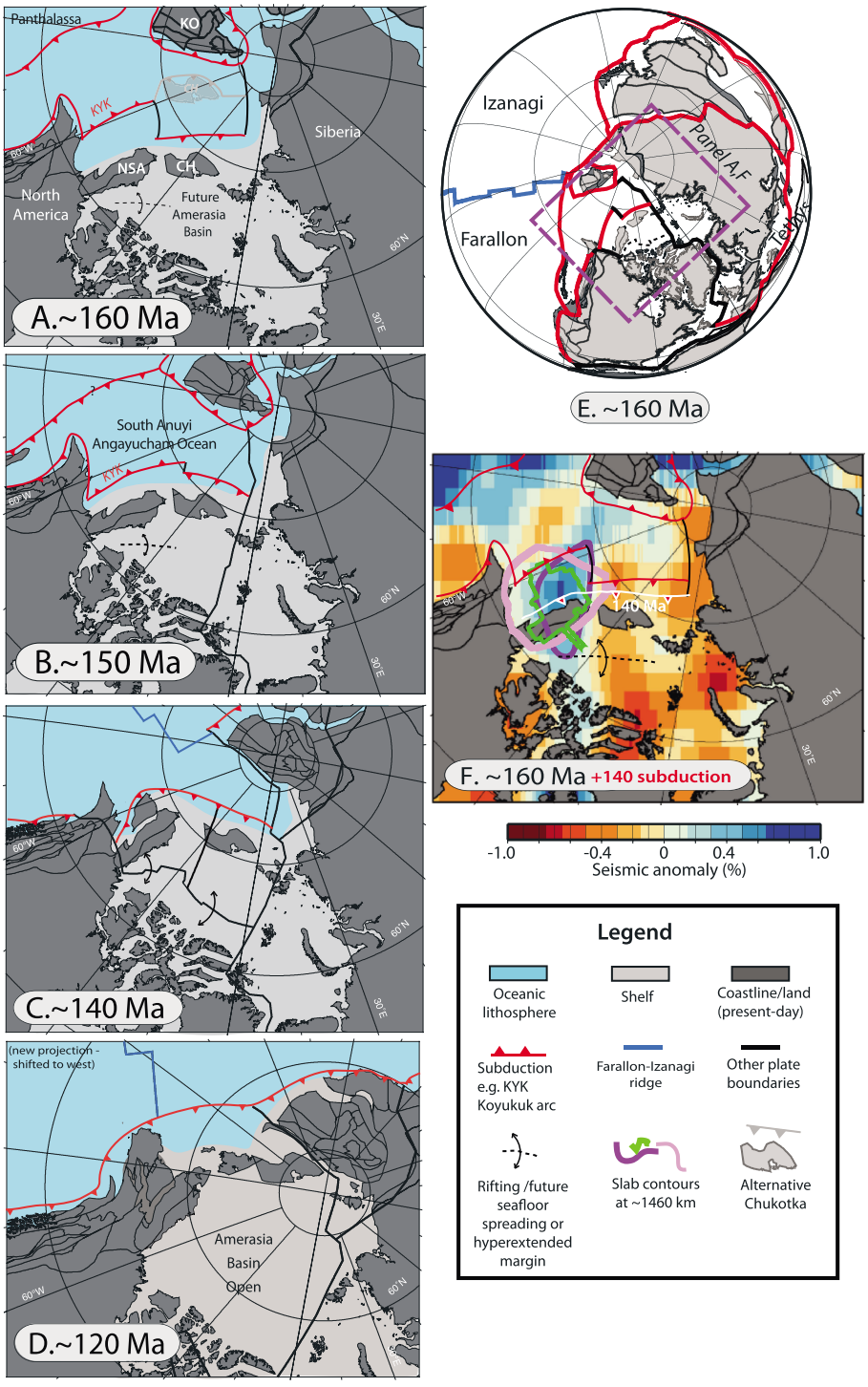

Figure 2. (a–d) Plate reconstructions at 160–120 Ma (adapted from *Shephard et al.* [2013]), around the onset of South Anuyi-Angayucham Ocean subduction, rotation of the North Slope and Chukotka, and opening of the Amerasia Basin. See inset legend for details. CH: Chukotka, KO: Kolyma-Omolon terrane, NSA: North Slope of Alaska. Light grey block and subduction at 160 Ma show approximate location of Chukotka in alternative models [e.g., *Amato et al.*, 2015] (Figure S12) and separation into two ocean basins. (e) Zoom-out showing Arctic in broader context at 160 Ma. (f) As in Figure 2a but underlain by seismic tomography model S40RTS (1460 km; contours as in Figures 1 and 3) showing Greenland slab in relation to overlying subduction zones, also at 140 Ma related to Amerasia Basin opening. Successive episodes of regional subduction with variable polarity and trench motion, rather than a singular event, may account for the seismic anomaly.

The incessant recycling of oceanic lithosphere by subduction means that only limited information about the age and structure of subducted oceans can be inferred from the few preserved sutures and ophiolitic complexes. Sparse or inaccessible outcrops and ambiguous paleomagnetic and geological data prove insufficient for recreating the detailed history of the South Anuyi-Angayucham Ocean; thus, complementary data sets and methods must be sought. One such approach is the joint analysis of regional tectonic data, kinematic plate models, and tomographic images, which not only integrate horizontal plate movements but also track subducted mantle material [e.g., *van der Meer et al*., 2010]. Following this approach, *Shephard et al*. [2013] mapped mantle provinces in tomographic models available for the Arctic and correlated them with specific subduction episodes. Among these regional positive velocity anomalies, one located ~1000–1600 km under present-day Greenland was noted. Based on a vertical correlation to paleosubduction zones, this mid-mantle anomaly was tentatively linked to paleo-Arctic subduction and, furthermore, could be broadly reproduced by coupled plate motion-mantle convection models [*Shephard et al*., 2014]. Here we explore available complementary evidence to support the existence of this distinct slab and evaluate its broader geodynamic implications over time.

2. Seismic Tomography

Seismic tomography models, based on *P* and/or *S* waves, image mantle anomalies which have relatively faster or slower velocities compared to depth-averaged mantle models. Faster anomalies are generally assigned to colder than ambient mantle material and are identified as subducted lithosphere. Efforts to link subduction history to surface kinematics using slabs imaged by seismic tomography have been undertaken on global [e.g., *van der Meer et al*., 2010, 2012] and regional scales [e.g., *Schellart and Spakman*, 2015] including the Arctic [*Shephard et al*., 2013; *Gaina et al*., 2014].

We focus on a distinct fast seismic feature in the mid-mantle, under present-day Greenland (Figure 1), visible in cross sections across several global tomography models (Figures 3 and S1–S3), including S40RTS [*Ritsema et al*., 2011], UU-P07 [*Amaru*, 2007], and GyPSuMS [*Simmons et al*., 2010] (*Grand* [2002] in the supporting information). The two models, S40RTS and UU-P07, are independent of each other and therefore are well suited to evaluate the robustness of a particular seismic anomaly of being an image of actual mantle structure. This Greenland anomaly ranges between ~1000 and 1600 km depth and has a peak in amplitude around 1400 km and an approximate center point of 50°W, 65°N (Table S1). A fast tomographic anomaly of unknown origin in the transition zone is imaged above this region, although not shared in all tomography models. We cannot exclude that part of the slab has stagnated (see sinking rate discussion for further analysis).

With model and depth-dependent variation, the anomaly is characterized by both subrounded and elongate geometries (Figure 3). Limited depth slices show a NW-SE elongation of the anomaly; however, considering its mid-mantle location, any relation to surface trench motions is not clear. The depth and location of the proposed slab from tomography are complicated by the subduction history, sinking behavior and associated advection and interaction with regional mantle flow. Nonetheless, the match between the mantle anomaly identified in tomography and surface kinematic reconstructions (i.e., absolute reference frame and assuming near vertical sinking) points to the South Anuyi-Angayucham Ocean.

The Greenland anomaly is separated from the deeper and prominent "Farallon slab," located farther west, by a region of negative (slow) seismic anomalies [e.g., *Grand et al*., 1997; *Sigloch et al*., 2008] (Figures 3, S1, and S2). The Farallon slab is considered to be related to subduction along North America from 100 Ma [*Grand et al*., 1997] or to intraoceanic subduction within northeast Panthalassa (Figure 2) [*Sigloch and Mihalynuk*, 2013]. The latter scenario might account for at least the northern portion of the Farallon slab which matches a long-lived Panthalassa subduction zone that existed far outboard of the South Anuyi-Angayucham Ocean (Figure 2). In combination with UU-P07 resolution tests (Figure S4; see *Hall and Spakman* [2015] for more information and quality assessment), this suggests a spatially separate and discrete subduction history for the Greenland anomaly and supports our paleo-Arctic interpretation. Other known Late Jurassic paleosubduction regions, namely, the Tethys, are too remote and could not account for the sub-Greenland slab. Improved resolution of both surface data sets and mantle tomography models may shed light on finer regional tectonic details.

3. Sinking Rates

To place the observed Greenland anomaly in a kinematic context, we explore a circum-Arctic plate reconstruction and assess the correlation between the age and depth of the inferred slab and the sinking rates.

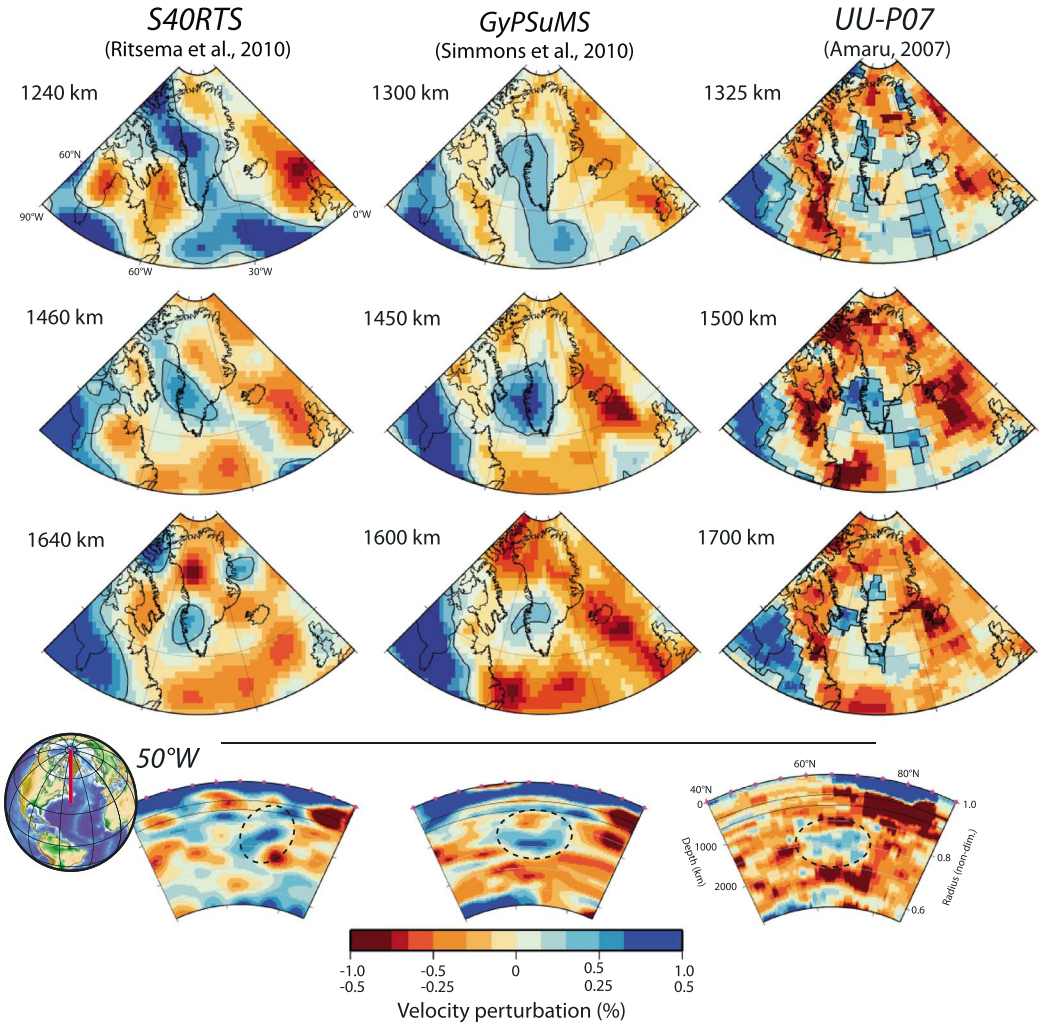

Figure 3. Horizontal slices ranging from ~1300 to 1600 km and vertical slices (50°W, 40–90°N, globe inset) through seismic tomography models S40RTS [*Ritsema et al*., 2011], GyPSuMS [*Simmons et al*., 2010], and UU-P07 [*Amaru*, 2007], half color scale due to model scaling. Black contour in horizontal slices identifies approximate slab edge based on the 0.3% seismic contour (0.15% UU-P07). Additional depths and *Grand* [2002] in Figures S1–S3.

In a fixed mantle frame, the mantle region under present-day Greenland was overlain by the Arctic and northernmost Panthalassa during the Mesozoic (Figure 2) [*Shephard et al*., 2013].

A dual sinking rate and slab subduction age approach (Table S2) is appropriate when the age of subduction is not well constrained by the geological record, as is the case in frontier regions such as the Arctic. Inferred sinking rates represent the averages of higher sinking rates in the low-viscosity upper mantle and transition zone, possible slab stagnation around 660 km and lower rates in the high-viscosity lower mantle [e.g., *Goes et al*., 2008; *Ricard et al*., 1993; *Steinberger and Calderwood*, 2006]. Notably, several recent studies present observational and experimental evidence for a strong viscosity gradient through the uppermost 300–500 km of the lower mantle, with a maximum at about 1000 km depth (800–1200 km) [*Fukao and Obayashi*, 2013; *Ballmer et al*., 2015; *French and Romanowicz*, 2015; *Marquardt and Miyagi*, 2015; *Rudolph et al*., 2015] (Figure 5c). Additional slab stagnation near the 660 km discontinuity may be due to endothermic transition from ringwoodite to a bridgemanite-dominated mineral assemblage and pyroxene and/or olivine metastability, especially in cold subduction zones [*King et al*., 2015; *Simmons et al*., 2015]. The high seismic velocity in the transition zone in two of the tomographic models (Figure 2) may explain slab remnants from the latest phase of subduction and supports our use of a globally averaged sinking rate.

Assuming vertical slab sinking and a slab base of 1600 km depth, a globally averaged sinking rate of 1.2 (±0.3) cm/yr [*van der Meer et al*., 2010; *Butterworth et al*., 2014] implies a subduction age at the trench of ~133 (range 177–106) Ma (Table S2). Conversely, applying a subduction age of 160 and 120 Ma to a 1600 km slab yields sinking rates of 1 and 1.3 cm/yr, respectively. This sinking rate/age estimate supports the known geological record of the South Anyui-Angayucham suture(s) and existence of an Arctic paleo-ocean. Final stages of South Anuyi-Angayucham Ocean subduction correlate with a Late Jurassic-Early Cretaceous timing of Amerasia Basin opening. Notably, slightly slower rates inferred by ~160 Ma subduction timing (e.g., 1 cm/yr for slab at 1600 km; Table S2) are still consistent with the estimates (1.2 ± 0.3 cm/yr) and concur with the recent observations of regional subduction in which slab rollback considerably slows down the overall sinking rate [*Simmons et al*., 2015]. Such a low rate may concur with the sinking of a relatively small slab volume (as imaged in tomography and based on the plate reconstruction), which may increase the thermal absorption and reduce the negative slab buoyancy and sinking speed. Furthermore, a significantly younger age of final South Anuyi-Angayucham subduction (younger than ~120 Ma), and consequently, a faster sinking rate conflicts with overriding location of the continents (i.e., no overriding oceans) at younger times, regardless of absolute reference frame (Figures 2 and S5 and Table S2).

4. Gravity Gradients

To further evaluate the existence of the Greenland anomaly, we investigate gravity gradient data from the GOCE (Gravity field and steady-state Ocean Circulation Explorer) satellite mission [*Johannessen et al*., 2003; *Rummel et al*., 2011]. Gravity gradients are highly sensitive to the geometry of anomalous bodies at depth, and we map the gravity vector variations in different directions. These second-order derivatives of the gravitational potential are thus well suited for elucidating longitudinally or latitudinally striking features such as slab remnants. Long-wavelength nonhydrostatic gravity gradient anomalies at satellite altitude (225–255 km) reflect 3-D mass heterogeneities within Earth's mantle and induced density interface deflections, including down to mid-mantle depths for a thin, vertically sinking slab, and to the deep mantle for wider mass anomalies [*Panet et al*., 2014]. At large scales, gradient anomalies coincide with regions of long-lived subduction and deep-seated convective instabilities/plumes [*Panet et al*., 2014]. The sign of the gradient anomalies changes with the source depth, and fine-scale oscillations can occur above the edges of the mass anomaly, if its width-to-depth ratio is high enough, which puts stronger constraints on the source than geoid or gravity anomaly data. Difficulties in scaling seismic velocity to density make this global gravity data set a valuable addition in deciphering mantle structure.

We present a regional analysis of these gravity gradients at intermediate wavelengths relevant for our purpose (Figure 4, 1300 and 1500 km; 800 km and additional directions, Figure S6). The coordinates (r, θ, and ϕ) are the usual spherical coordinates corresponding to the (e_r, e_θ, and e_φ) local frame, where e_r is pointing radially outward, e_θ is pointing toward the south, and e_φ toward the east. Direction "$\phi\phi$" is the second derivative in the E-W direction and reveals N-S trending anomalies, "$\theta\theta$" is second derivative in N-S direction highlighting E-W trending mass anomalies, respectively, while "*rr*" is the second derivative in the radial direction. We observe a negative gravity gradient anomaly in the $\phi\phi$ component, and $\theta\theta$ to a lesser extent, focused on Baffin Bay and southern Greenland, pointing to mass excess, as well as a positive (negative in "*rr*") anomaly on Baffin Island. Modeling results of a 1000 × 500 km cylindrical anomaly (density contrast 80 kg/m^3 relative to preliminary reference Earth model) between 1000 and 1500 km depth matches the magnitude and location of the gravity gradients, particularly for the $\phi\phi$ component (see supporting information, Figure S6, and Table S3). These gravity perturbations correspond with the slab location from tomography and provide additional support for a positive density anomaly under Greenland.

5. Possible Interactions With the High Arctic Large Igneous Province

The Cretaceous was a period of widespread Arctic magmatism identified in Franz Josef Land, Sverdrup Basin, De Long Islands, Svalbard, and North Greenland (Figures 1 and 5b, e.g., *Morgan* [1983] and *Tarduno et al*. [1998]). Often referred to as the High Arctic Large Igneous Province (HALIP), magmatism is thought to have formed in several stages ranging from ~130–80 Ma, although shorter-lived (~124–122 Ma) [*Corfu et al*., 2013] timings have been proposed for different locations. The origins of HALIP magmatism are unclear and possible links to deep mantle plumes (Figure 5) or global mantle overturn are tenuous [e.g., *Larson*, 1991;

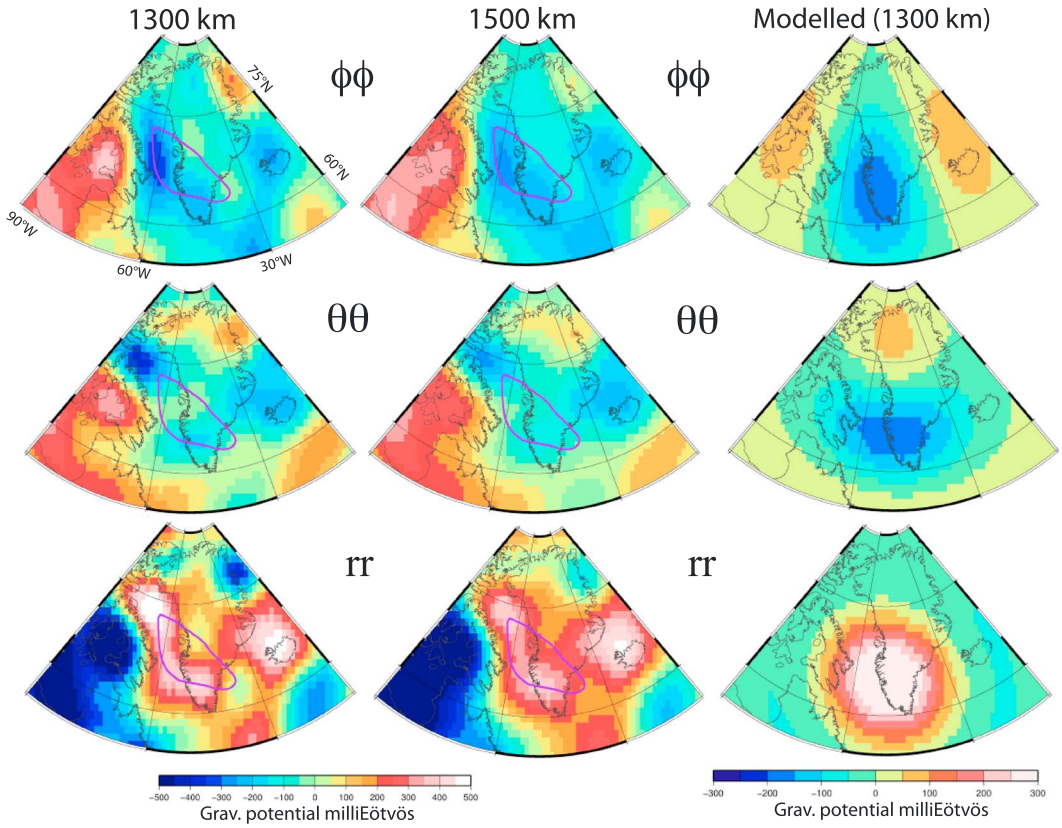

Figure 4. Gravity gradients [*Panet et al.*, 2014] filtered for 1300 and 1500 km wavelengths [*Panet et al.*, 2014] (800 km and additional directions in the supporting information and Figure S6), overlain with coastlines and S40RTS slab contour (Figure 2). Rightmost column shows forward-modeled gravity signal at the 1300 km wavelength (500 × 1000 km cylinder, 80 kg/m^3 density contrast). Gravity directions $\phi\phi$, $\theta\theta$, and *rr* highlight mantle mass features which show N-S, E-W, and radial variations, respectively.

Lawver and Müller, 1994; *Smirnov and Tarduno*, 2000]. Although the temporally and spatially overlapping events of Amerasia Basin opening, South Anuyi-Angayucham subduction and HALIP eruption appear related; geodynamic and geochemical relationships between them have not been established.

Geochemically characterized HALIP basaltic rocks from the Sverdrup Basin include 130–80 Ma tholeiitic rocks at Ellef Ringnes and Axel Heiberg islands and 85–60 Ma mildly alkaline basaltic rocks at Ellesmere Island [*Estrada*, 2014; *Evenchick et al.*, 2015; *Jowitt et al.*, 2014]. Franz Josef Land (FJL) basalts are also tholeiitic [*Ntaflos and Richter*, 2003] and generally more primitive than the basaltic rocks of the Sverdrup Basin.

Paleogeographic reconstructions of the Sverdrup Basin, combined with the imaged sub-Greenland slab and inferred subduction zone positions (Figures 2, 5, and S5), indicate that the HALIP melting region under the Sverdrup Basin at about 120 Ma may have coincided with the arc and back-arc mantle related to ~160–120 Ma South Anuyi-Angayucham subduction. Suprasubduction asthenosphere affected by the infiltration of fluids and melts from the breakdown of hydrous minerals and carbonates will acquire chemical signatures characteristic of many of the Sverdrup Basin HALIP basaltic rocks, especially the tholeiites from Ellef Ringnes and Axel Heiberg islands. These signatures include the elevated ratios of Pb/(Ce + Pr), Rb/Ba, and (Th + U)/(Nb + Ta) observed in normalized trace element diagrams (spider diagrams Figure 5a).

A preexisting arc or back-arc mantle from South Anuyi-Angayucham subduction could partly mix with and contaminate material supplied by a deep plume-type upwelling before or during shallow asthenospheric melting, resulting in the HALIP magmas. An average of samples from Heimaey in the Southern Volcanic Flank Zone of Iceland is included in Figure 5a as an example of a deep plume source with a considerable proportion of recycled oceanic crust (ROC). In contrast to the enriched tholeiitic rocks from Ellef Ringnes and Axel Heiberg islands, the Heimaey basalts are characterized by low ratios of Pb/(Ce + Pr), Rb/Ba, and (Th + U)/(Nb + Ta), as well

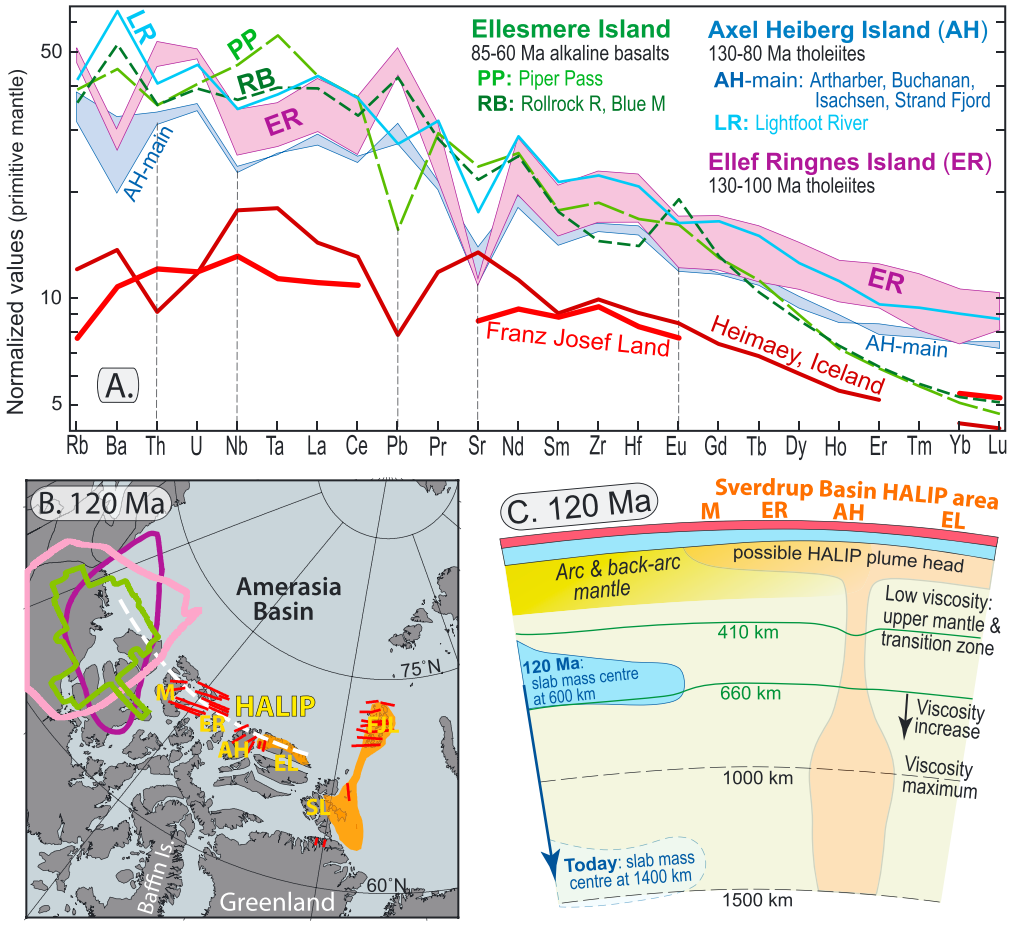

Figure 5. (a) Trace element concentrations normalized to primitive mantle [*Sun and McDonough*, 1989] for HALIP basaltic rocks from Ellef Ringnes [*Evenchick et al.*, 2015], Ellesmere and Axel Heiberg islands [*Jowitt et al.*, 2014; *Estrada*, 2014], and Franz Josef Land [*Ntaflos and Richter*, 2003]. The fields and lines representing the HALIP units are averages and ranges specified in Figures S7–S9. Samples from the Vestmanaeyjar system (Heimaey, Iceland) with a strong recycled oceanic lithosphere signature are included for comparison [*Peate et al.*, 2010]. After removal of the evolved and fractionated samples with <4.5 wt % MgO, the rocks from the same formations and areas were grouped and averaged (supporting information). (b) ~ 120 Ma plate reconstruction, coeval with major HALIP activity at Ellef Ringnes and Axel Heiberg Island. Dykes and volcanic regions are in red and orange. AH, EL, ER, and M: Axel Heiberg, Ellesmere, Ellef Ringnes, and Melville islands, respectively; FJL: Franz Josef Land; SL: Svalbard. Purple/green lines show the approximate slab extent (Figure 1), thick white line is trace of vertical section C. (c) Schematic model at 120 Ma. The arc and back-arc mantle affected by supra-subduction fluid and melt infiltration processes, and a possible HALIP-related plume is indicated.

as lower concentrations of most of the trace elements. In spite of incomplete data coverage, the HALIP basalts from FJL appear to be relatively similar to, and even less enriched than the Heimaey basalts. Based on the trace element patterns, arc or back-arc mantle contributions to the FJL basalts are therefore unlikely. The 120 Ma paleogeographic reconstructions and the schematic vertical section (Figures 2, 5b, and 5c) supports the notion that the 130–80 Ma tholeiitic rocks at Ellef Ringnes and Axel Heiberg islands are most likely to be affected by arc and back-arc mantle sources.

The elevated Sr/(Pr + Nd) ratios in the Heimaey basalts compared to all of the HALIP rocks in Figure 5a is due to assimilation of some gabbroic rocks from the thick and young oceanic basement crust generated in the Icelandic rift zone. The opposite process of plagioclase fractionation can explain the common Sr depletion in the HALIP basaltic rocks and in many other evolved basaltic suites.

Unfortunately, the arc-type chemical signature of most of the tholeiites from Ellef Ringnes and Axel Heiberg is not unambiguous and could potentially be related to contamination with upper continental crust (UCC). Considerable amounts of UCC contamination, however, are likely to impose heterogeneities between and

within individual magma batches. A more complete discussion of the chemical variability of the HALIP basalts and the possibilities of UCC contamination is provided as supporting information.

In summary, geochemical features indicate that several of the 130–80 Ma tholeiitic rocks from Ellef Ringnes and Axel Heiberg islands, which at eruption times were closest to the former South Anuyi-Angayucham subduction, may have incorporated significant amounts of arc and back-arc mantle. Although a clear discrimination between arc-like mantle sources and upper crustal contamination is difficult, we find that some of the distinct trace element concentration patterns across the different volcanic and subvolcanic units may have resulted from arc-like mantle sources associated with the South Anuyi-Angayucham slab(s). Trace element patterns in the HALIP basalts in the Sverdrup Basin suggest that suprasubduction, arc-type mantle might have mixed with plume-supplied material.

6. Conclusions

Independent *P* and *S* wave tomography models image a distinct, mid-mantle (1000–1600 km) positive seismic anomaly under present-day Greenland, which is spatially linked to perturbations in gravity gradients. We interpret the mantle anomaly as a remnant of subduction. Using plate reconstructions in a mantle reference frame and assuming vertical slab sinking, we link the position of this anomaly to the closure of the South Anuyi-Angayucham Ocean. Final stages of regional subduction were likely linked to the complementary opening of the Amerasia Basin. Consistent with a range of whole-mantle sinking rates (1.2 ± 0.3 cm/yr) and evidence from the geological record, the slabs were likely subducted in the Late Jurassic-Early Cretaceous. Although minor crustal contamination is likely, HALIP geochemistry in the Sverdrup Basin seems to incorporate arc-mantle sources, bringing the origin of the HALIP a step further to resolution. The combination of seismic tomography, satellite gravimetry, and plate reconstructions shed new light on the mantle evolution under present-day Greenland.

Acknowledgments

G.E.S., R.G.T., W.S., and C.G. acknowledge support from the Research Council of Norway through its Centres of Excellence funding scheme, project 22372. I.P. acknowledges CNES for financial support through the TOSCA committee. Data supporting the conclusions can also be obtained in the supporting information. We thank Marianne Greff-Lefftz for computing the gravity modeling. We would like to thank the Editor Michael Wysession, as well as Nathan Simmons and an anonymous reviewer for their helpful comments that improved the manuscript. We also thank Elizabeth Miller for advice on an earlier version of the manuscript.

References

Alvey, A., C. Gaina, N. J. Kusznir, and T. H. Torsvik (2008), Integrated crustal thickness mapping and plate reconstructions for the high Arctic, *Earth Planet. Sci. Lett.*, *274*(3–4), 310–321.

Amaru, M. L. (2007), Global travel time tomography with 3-D reference models, *Geol. Ultraiectina*, *274*, 174.

Amato, J. M., J. Toro, V. V. Akinin, B. A. Hampton, A. S. Salnikov, and M. I. Tuchkova (2015), Tectonic evolution of the Mesozoic South Anyui suture zone, eastern Russia: A critical component of paleogeographic reconstructions of the Arctic region, *Geosphere*, *11*(5), 1530, doi:10.1130/GES01165.1.

Ballmer, M. D., N. C. Schmerr, T. Nakagawa, and J. Ritsema (2015), Compositional mantle layering revealed by slab stagnation at ~1000-km depth, *Sci. Adv.*, *1*, e1500815.

Butterworth, N. P., A. S. Talsma, R. D. Müller, M. Seton, H.-P. Bunge, B. S. A. Schuberth, G. E. Shephard, and C. Heine (2014), Geological, tomographic, kinematic and geodynamic constraints on the dynamics of sinking slabs, *J. Geodyn.*, *73*, 1–13.

Corfu, F., S. Polteau, S. Planke, J. I. Faliede, H. Svenson, A. Zayoncheck, and N. Stolbov (2013), U-Pb geochronology of Cretaceous magmatism on Svalbard and Franz Josef Land, Barents Sea Large Igneous Province, *Geol. Mag.*, *150*(06), 1127–1135.

Domeier, M., and T. H. Torsvik (2014), Plate tectonics in the late Paleozoic, *Geosci. Front.*, *5*(3), 303–350.

Drachev, S. S., L. A. Savostin, V. G. Groshev, and I. E. Bruni (1998), Structure and geology of the continental shelf of the Laptev Sea, Eastern Russian Arctic, *Tectonophysics*, *298*(4), 357–393.

Estrada, S. (2014), Geochemical and Sr–Nd isotope variations within Cretaceous continental flood-basalt suites of the Canadian High Arctic, with a focus on the Hassel Formation basalts of northeast Ellesmere Island, *Int. J. Earth Sci.*, doi:10.1007/s00531-014-1066-x.

Evenchick, C. A., W. J. Davis, J. H. Bédard, N. Hayward, and R. M. Friedman (2015), Evidence for protracted High Arctic large igneous province magmatism in the central Sverdrup Basin from stratigraphy, geochronology, and paleodepths of saucer-shaped sills, *Geol. Soc. Am. Bull.*, *127*, 1366.

French, S. W., and B. Romanowicz (2015), Broad plumes rooted at the base of the Earth's mantle beneath major hotspots, *Nature*, *525*, 95–99.

Fukao, Y., and M. Obayashi (2013), Subducted slabs stagnant above, penetrating through, and trapped below the 660 km discontinuity, *J. Geophys. Res. Solid Earth*, *118*, 5920–5938, doi:10.1002/2013JB010466.

Gaina, C., S. Medvedev, T. Torsvik, I. Koulakov, and S. Werner (2014), 4D Arctic: A glimpse into the structure and evolution of the Arctic in the light of new geophysical maps, plate tectonics and tomographic models, *Surv. Geophys.*, *35*(5), 1095–1122.

Goes, S., F. A. Capitanio, and G. Morra (2008), Evidence of lower-mantle slab penetration phases in plate motions, *Nature*, *451*, 981–984.

Grand, S. P. (2002), Mantle shear-wave tomography and the fate of subducted slabs, *Philos. Trans. R. Soc. A*, *360*, 2475–2491.

Grand, S. P., R. D. van der Hilst, and S. Widiyantoro (1997), Global seismic tomography: A snapshot of convection in the Earth, *GSA Today*, *7*(4), 1–7.

Grantz, A., P. E. Hart, and V. A. Childers (2011), Chapter 50: Geology and tectonic development of the Amerasia and Canada Basins, Arctic Ocean, *Geol. Soc. London Mem.*, *35*(1), 771–799.

Hall, R., and W. Spakman (2015), Mantle structure and tectonic history of SE Asia, *Tectonophysics*, *658*, 14–45.

Johannessen, J. A., et al. (2003), The European Gravity Field and steady-state Ocean Circulation Explorer satellite mission its impact on geophysics, *Surv. Geophys.*, *24*(4), 339–386.

Jowitt, S. M., M.-C. Williamson, and R. E. Ernst (2014), Geochemistry of the 130 to 80 Ma Canadian High Arctic Large Igneous Province (HALIP) event and implications for Ni-Cu-PGE prospectivity, *Econ. Geol.*, *109*(2), 281–307.

King, S. D., D. J. Frost, and D. C. Rubie (2015), Why cold slabs stagnate in the transition zone, *Geology*, *43*, 231–234.

Larson, R. L. (1991), Geological consequences of superplumes, *Geology*, *19*, 963–966.
Lawver, L. A., and R. D. Müller (1994), Iceland hotspot track, *Geology*, *22*(4), 311–314.
Lawver, L. A., A. Grantz, and L. M. Gahagan (2002), Plate kinematic evolution of the present Arctic region since the Ordovician, in *Tectonic Evolution of the Bering Shelf–Chukchi Sea–Arctic Margin and Adjacent Landmasses*, edited by E. L. Miller, A. Grantz, and S. L. Klemperer, *Geol. Soc. Am. Spec. Pap.*, *360*, 333–358.
Marquardt, H., and L. Miyagi (2015), Slab stagnation in the shallow lower mantle linked to an increase in mantle viscosity, *Nat. Geosci.*, *8*, 311–314.
Miller, E. L., J. Toro, G. Gehrels, J. M. Amato, A. Prokopiev, M. I. Tuchkova, V. V. Akinin, T. A. Dumitru, T. E. Moore, and M. P. Cecile (2006), New insights into Arctic paleogeography and tectonics from U-Pb detrital zircon geochronology, *Tectonics*, *25*, TC3013, doi:10.1029/2005TC001830.
Miller, E. L., S. M. Katkov, A. Strickland, J. Toro, V. Akinin, and T. A. Dumitru (2009), Geochronology and thermochronology of Cretaceous plutons and metamorphic country rocks, Anyui-Chukotka fold belt, northeastern Arctic Russia, in *Geology, Geophysics and Tectonics of Northeastern Russia: A Tribute to Leonid Parfenov*, *Stephan Mueller Spec. Publ. Ser.*, vol. 4, edited by D. B. Stone et al., pp. 223–241, European Geophysical Union, Copernicus GmbH, Göttingen Germany.
Miller, E. L., G. Gehrels, V. Pease, and S. Sokolov (2010), Stratigraphy and U-Pb detrital zircon geochronology of Wrangel Island, Russia: Implications for Arctic paleogeography, *AAPG Bull.*, *94*(5), 665–692.
Miller, E. L., A. V. Soloviev, A. Prokopiev, J. Toro, D. Harris, A. B. Kuzmichev, and G. E. Gehrels (2013), Triassic river systems and the paleo-Pacific margin of northwestern Pangea, *Gondwana Res.*, *23*, 1631–1645.
Moore, T. E., P. B. O'Sullivan, C. J. Potter, and R. A. Donelick (2015), Provenance and detrital zircon geochronologic evolution of lower Brookian foreland basin deposits for the western Brooks Range, Alaska, and implications for early Brookian tectonics, *Geosphere*, *11*(1), 1–30.
Morgan, W. J. (1983), Hotspot tracks and the early rifting of the Atlantic, in *Developments in Geotectonics*, edited by P. Morgan and B. H. Baker, pp. 123–139, Elsevier, Amsterdam.
Nokleberg, W. J., L. M. Parfenov, J. W. H. Monger, I. O. Norton, A. I. Khanchuk, D. B. Stone, C. R. Scotese, D. W. Scholl, and K. Fujita (2000), Phanerozoic tectonic evolution of the circum-North Pacific, Professional Paper, 1626, 122 pp., *U.S. Geol. Surv*, *Washington*, *D. C.*
Ntaflos, T., and W. Richter (2003), Geochemical constraints on the origin of the continental flood basalt magmatism in Franz Josef Land, Arctic Russia, *Eur. J. Mineral.*, *15*(4), 649–663.
Panet, I., G. Pajot-Metivier, M. Greff-Lefftz, L. Metivier, M. Diament, and M. Mandea (2014), Mapping the mass distribution of Earth's mantle using satellite-derived gravity gradients, *Nat. Geosci.*, *7*(2), 131–135.
Peate, D. W., K. Breddam, J. A. Baker, M. D. Kurz, A. K. Barker, T. Prestvik, N. Grassineau, and A. C. Skovgaard (2010), Compositional characteristics and spatial distribution of enriched Icelandic mantle components, *J. Petrol.*, *51*(7), 1447–1475.
Ricard, Y., M. Richards, C. Lithgow-Bertelloni, and Y. Le Stunff (1993), A geodynamic model of mantle density heterogeneity, *J. Geophys. Res.*, *98*(B12), 21,895–21,909, doi:10.1029/93JB02216.
Ritsema, J., A. Deuss, H. J. van Heijst, and J. H. Woodhouse (2011), S40RTS: A degree-40 shear-velocity model for the mantle from new Rayleigh wave dispersion, teleseismic traveltime and normal-mode splitting function measurements, *Geophys. J. Int.*, *184*(3), 1223–1236.
Rowley, D. B., and A. L. Lottes (1988), Plate-kinematic reconstructions of the North Atlantic and Arctic: Late Jurassic to present, *Tectonophysics*, *155*(1–4), 73–120.
Rudolph, M. L., V. Lekic, and C. Lithgow-Bertelloni (2015), Viscosity jump in Earth's mid-mantle, *Science*, *350*, 1349–1352.
Rummel, R., W. Yi, and C. Stummer (2011), GOCE gravitational gradiometry, *J. Geod.*, *85*(11), 777–790.
Schellart, W. P., and W. Spakman (2015), Australian plate motion and topography linked to fossil New Guinea slab below Lake Eyre, *Earth Planet. Sci. Lett.*, *421*, 107–116.
Seton, M., et al. (2012), Global continental and ocean basin reconstructions since 200 Ma, *Earth Sci. Rev.*, *113*(3–4), 212–270.
Shephard, G. E., R. D. Müller, and M. Seton (2013), The tectonic evolution of the Arctic since Pangea breakup: Integrating constraints from surface geology and geophysics with mantle structure, *Earth Sci. Rev.*, *124*, 148–183.
Shephard, G. E., N. Flament, S. Williams, M. Seton, M. Gurnis, and R. D. Müller (2014), Circum-Arctic mantle structure and long-wavelength topography since the Jurassic, *J. Geophys. Res. Solid Earth*, *119*, 7889–7908, doi:10.1002/2014JB011078.
Sigloch, K., and M. G. Mihalynuk (2013), Intra-oceanic subduction shaped the assembly of Cordilleran North America, *Nature*, *496*(7443), 50–56.
Sigloch, K., N. McQuarrie, and G. Nolet (2008), Two-stage subduction history under North America inferred from multiple-frequency tomography, *Nat. Geosci.*, *1*(7), 458–462.
Simmons, N. A., A. M. Forte, L. Boschi, and S. P. Grand (2010), GyPSuM: A joint tomographic model of mantle density and seismic wave speeds, *J. Geophys. Res.*, *115*, B12310, doi:10.1029/2010JB007631.
Simmons, N. A., C. S. Myers, G. Johannesson, E. Mazel, and S. P. Grand (2015), Evidence for long-lived subduction of an ancient tectonic plate beneath the southern Indian Ocean, *Geophys. Res. Lett.*, *42*, 9270–9278, doi:10.1002/2015GL066237.
Smirnov, A. V., and J. A. Tarduno (2000), Low-temperature magnetic properties of pelagic sediments (Ocean Drilling Program Site 805C): Tracers of maghemitization and magnetic mineral reduction, *J. Geophys. Res.*, *105*(B7), 16,457–16,471, doi:10.1029/2000JB900140.
Sokolov, S. D., G. Y. Bondarenko, O. L. Morozov, V. A. Shekhovtsov, S. P. Glotov, A. V. Ganelin, and I. R. Kravchenko-Berezhnoy (2002), South Anyui suture, northeast Arctic Russia: Facts and problems, *Geol. Soc. Am. Spec. Pap.*, *360*, 209–224.
Steinberger, B., and A. R. Calderwood (2006), Models of large-scale viscous flow in the Earth's mantle with constraints from mineral physics and surface observations, *Geophys. J. Int.*, *167*(3), 1461–1481.
Sun, S.-S., and W. F. McDonough (1989), Chemical and isotopic systematics of oceanic basalts: Implications for mantle composition and processes, *Geol. Soc. London Spec. Publ.*, *42*(1), 313–345.
Tarduno, J. A., D. B. Brinkman, P. R. Renne, R. D. Cottrell, H. Scher, and P. Castillo (1998), Evidence for extreme climatic warmth from Late Cretaceous Arctic vertebrates, *Science*, *282*(5397), 2241–2243.
Till, A. B. (2016), A synthesis of Jurassic and Early Cretaceous crustal evolution along the southern margin of the Arctic Alaska-Chukotka microplate and implications for defining tectonic boundaries active during opening of Arctic Ocean basins, *Lithosphere, Geol. Soc. Am.*, doi:10.1130/L471.1.
Toro, J., J. M. Amato, and B. Natal'in (2003), Cretaceous deformation, Chegitun River area, Chukotka Peninsula, Russia: Implications for the tectonic evolution of the Bering Strait region, *Tectonics*, *22*(3), 1021, doi:10.1029/2001TC001333.
van der Meer, D. G., W. Spakman, D. J. J. van Hinsbergen, M. L. Amaru, and T. H. Torsvik (2010), Towards absolute plate motions constrained by lower-mantle slab remnants, *Nat. Geosci.*, *3*(1), 36–40.
van der Meer, D. G., T. H. Torsvik, W. Spakman, D. J. J. van Hinsbergen, and M. L. Amaru (2012), Intra-Panthalassa Ocean subduction zones revealed by fossil arcs and mantle structure, *Nat. Geosci.*, *5*(3), 215–219.

Supplementary Methods and Figures for:

Evidence for slab material under Greenland and links to Cretaceous High Arctic magmatism

G.Shephard, R.G. Trønnes, W. Spakman, I. Panet, C. Gaina

Tomography models and sinking rates

Tomography model *S40RTS* (Ritsema et al., 2011) is a global shear wave velocity model. Waveform anomalies were calculated via PREM (Dziewonski and Anderson, 1981) and datasets included Rayleigh wave phase delays, teleseismic body waves and normal mode splitting functions. Tomography model *UU-P07* (Amaru, 2007) is a P-wave model derived relative to the 1D reference model of ak135 (Kennett et al., 1995). Additional tomography models, including *GyPSuMS* (Simmons et al., 2010), based on body wave travel times and density datasets, and *Grand* (Grand, 2002) based only on shear body wave travel times, also show the proposed anomaly.

Table S1: Summary of identified Greenland anomaly feature according to alternative seismic tomography models:

Tomography model	**Contour value (%)**	**Longitudinal range (°W)**	**Latitudinal range (°N)**	**Depth range (km)**
Grand	*0.15*	*60-30*	*55-75*	*1000-1600*
GyPSuMS	*0.3*	*60-40*	*55-70*	*1200-1600*
S40RTS	*0.3*	*70-30*	*55-75*	*660-1700*
UU-P07	0.15	*65-45*	*60-70*	*1300-1700*

Table S2: Comparison of slab depth, sinking rates and age of subduction at the trench.

Slab depth	**Assumption**	**Corresponding age/sinking rate**
1400 km (mid point)	120 Ma	1.2 cm/yr
	160 Ma	0.9 cm/yr
	@ 1.2 cm +/- 0.3 /yr	116 Ma (range 93-155 Ma)
	@ 2 cm/yr	70 Ma
1600 km (max. base)	120 Ma	1.3 cm/yr
	160 Ma	1 cm/yr
	@ 1.2 cm +/- 0.3 /yr	133 Ma (range 106-177 Ma)
	@ 2 cm/yr	80 Ma

Gravity

Our analysis of wavelengths of less than 1300 km (800 km, for example; Fig. S6) showed that the gravity gradient signal is likely complicated by the lithosphere and shallower mantle signals (for example the triplication is parallel to the edges of the continent-ocean boundary). We therefore only investigated larger wavelengths, of 1300 and 1500 km. To investigate the predicted signal of a slab feature at depth, we performed additional gravity calculations. A 1000 x 500 km elongated cylindrical anomaly (density contrast 80 kg/m^3 relative to PREM) located between 1000-1500 km depth was used to model the slab mass anomaly. Earth's deformations in response to this internal load were computed as in Panet et al. (2014), assuming a standard viscosity profile for oceans, with a low viscosity later below the lithosphere and a viscosity increase in the lower mantle (Table S3). The total gravity signal is obtained by summing the direct source attraction and the contribution from induced deformation. For the considered mass source, the deformations term is very small. Because of attenuation by upward continuation to the Earth's surface, the slab gravity signal at the Earth's surface is smooth and the source spatial shape is not well

resolved. This is due to the trade-off between source spatial extent and distance of observation, as a result, the 1500 km scale is found representative of the signal.

Table S3: Parameters for the forward gravity modelling

Depth	***Viscosity***
0-60 km	10^{22} *Pa.s*
60-160 km	10^{19} *Pa.s*
160-670 km	10^{20} *Pa.s*
670-1150 km	*linear increase*
1150 km – CMB	10^{22} *Pa.s*

Geochemistry

To evaluate the nature of the mantle sources and possible effect of crustal contamination on the magmas, we use normalized trace element concentration diagrams. Whereas Fig. S7 (and Fig. 5) show average trace element patterns of various sample suites, the individual HALIP samples are shown in six separate panels in Fig. S8 and S9. Samples with less than 4.5 wt% MgO are excluded, with the exception of the evolved high-phosphorus series of the Hassel formation.

Subducted slabs sinking below 100-200 km depth undergo devolatilization, resulting in metasomatic enrichments and partial melting in the mantle wedge (Hofmann, 1997; Poli and Schmidt 2002; Manning, 2004; Woo et al., 2014). The trace element are useful for discriminating between the complementary components of recycled oceanic crust (ROC) and arc mantle. ROC is characterized by high ratios of strongly to moderately high-field

strength elements (HFSE), e.g. (Nb+Ta)/(Th+U), high U/Pb (high-μ ratio, HIMU) and low Rb/Ba. The average of three Heimaey basalts from Peate et al. (2010), sampling the ROC (HIMU) component of the Iceland plume (e.g. Trønnes et al., 2013) is included as a reference pattern. In contrast to most mantle-derived magmas, Icelandic basalts have generally elevated Sr and Eu concentrations, acquired during the passage through voluminous gabbroic cumulates in the thick crust. Extensive fractionation of plagioclase from primitive magmas will, in contrast, lower Sr/(Pr+Nd) ratios, as seen in the HALIP samples. The FJL tholeiitic basalts are the HALIP rocks that most closely resemble the Heimaey alkaline basalts, although the latter are more enriched, with higher ratios of LREE/HREE (Light and Heavy Rare Earth Elements, respectively), indicating lower degrees of melting of a fertile mantle source with high (Nb+Ta)/(Th+U) ratio and therefore a high ROC proportion. Compared to the FJL basalts, the Sverdrup Basin rocks are more enriched and more evolved, with higher lithophile trace element contents and higher LREE/HREE ratios. Feldspar fractionation at shallow level and oxidizing conditions are indicated by Sr-depletion without corresponding Eu-depletion (normalized Sr/Nd and Eu/Gd ratios are 0.4-0.9 and 1.0-1.5, respectively). The mildly alkaline basaltic rocks from Ellesmere Island with the steepest REE patterns and low concentrations of the chalcophile elements like the platinum group elements (PGEs) might have formed by low-degree S-saturated melting, locking the PGEs into residual mantle sulphides (Jowitt et al. 2014). In contrast, the large degree tholeiitic magmas on Axel Heiberg Island were S-undersaturated and scavenged the chalcophiles from the mantle residue. Most of the tholeiitic and some of the mildly alkaline basalts from the Sverdrup Basin have high (Th+U)/(Nb+Ta) ratios and positive Pb-anomalies, characteristic of arc magmas (e.g. Keleman et al., 2003). The main unit with negative Pb-anomalies and low (Th+U) /Nb+Ta) ratios is the ROC-like alkaline Piper Pass basalts from the Ellesmere Island,

which is also the most enriched (e.g. the highest LREE/HREE ratios) of all the HALIP basalts. The tholeiitic Lightfoot River basalts from Axel Heiberg Island represent an intermediate case between ROC- and arc-like signatures.

Jowitt et al (2014) discussed possible scenarios of upper continental crust (UCC) contamination, partly based on the concentration of the chalcophile elements, especially the PGEs, Pt and Pd. They suggested that UCC contamination involved sulphur assimilation and saturation, and sulphide fractionation in the mildly alkaline magmas, resulting in reduced Pt and Pd. They also used elevated Th/Yb and reduced Nb/Th ratios as an additional UCC contamination indicator. Low PGE abundances in the Piper Pass and Lightfoot River basalts might suggest that these two units without arc mantle signature are more contaminated than other basalts from the Ellesmere and Axel Heiberg Islands, respectively. In that specific case, UCC contamination does not correspond to an arc- or backarc-like mantle chemistry. The suggested UCC contaminated Piper Pass unit has the highest La/Sm, Th/Yb and Nb/Ta ratios of all the basalts from the Sverdrup Basin and Franz Josef Land.

The arc-like positive Pb-anomalies and high (Th+U)/(Nb+Ta) ratios in most of the other Sverdrup Basin basaltic rocks could also be amplified by UCC assimilation. The high Rb/Ba ratios and the indications of elevated Zr and Hf concentrations in the tholeiitic rocks from Ellef Ringnes Island and most of the Bastion Ridge, Artharber Creek and Buchanan Lake tholeiitic rocks could possibly be ascribed to a UCC contribution (e.g. Rudnick and Gao, 2003, Fig. S10). In contrast, the mildly alkaline Rollrock River and Blue Mountain suites from Ellesmere Island have low Rb/Ba ratios and low concentrations of Zr and Hf, in addition to intermediate (Th-U)/(Nb+Ta) ratios. Similar

geochemical features, also reminiscent of lower continental crust, are distinct from an arc-mantle pattern. Significant amounts of UCC contamination will probably lead to pronounced chemical variation between individual magma batches. The larger heterogeneities observed within each of the sample suites from Axel Heiberg Island compared to those of the Ellesmere and Ellef Ringnes Islands (Fig. S8 and S9) might possibly be related to UCC contamination. In contrast to some of the inferences of Jowitt et al. (2014), Estrada (2015) concluded that the main geochemical features of the Ellesmere Island basaltic rocks are mantle source related even if limited continental crust assimilation can be recognized. The location of the Ellesmere Island area furthest away from the inferred South Anuyi trench, appears to be in agreement with the lack of distinct arc or back-arc mantle signature there. In spite of relatively high Pb/(Ce+Pr) ratios of the Rollrock River and Blue Mountain rock suites, they do not have elevated (Th+U)/(Nb+Ta) and Rb/Ba ratios.

The Rb/Ba and (Rb+Ba)/La ratios are more variable. The Buchanan Lake and Lightfoot River sample suites show the largest internal variation, e.g. in terms of the Rb/Ba and Pb/(Ce+Pr) ratios. Some of the scattered variation might be due to alteration and weathering processes and variable amounts of upper crustal contamination. To evaluate the relative importance of continental crust assimilation and arc mantle involvement in the melting zone of the HALIP magmas, we used trace element patterns of average upper and lower continental crust and continental and oceanic arc basalts (Fig. S10; Rudnick and Gao, 2003; Keleman et al. 2003). The elevated (Th+U)/(Nb+Ta) and Pb/(Ce+Pr) ratios of most of the Sverdrup Basin (SB) basaltic rocks are most likely caused by a combination of arc mantle and upper continental crust (UCC) involvement. Lower continental crust has generally too low (Th+U)/(Nb+Ta) ratio to be an appropriate candidate. The

consistently low Sr/(Pr+Nd) ratios of the Sverdrup Basin mafic rocks, which are not matched by correspondingly low Eu/Gd ratios, are probably caused by shallow-level feldspar fractionation under relatively oxidizing conditions with low Eu^{2+}/Eu^{3+} ratios, rather than by UCC contamination. Average UCC has possibly also too high (Zr+Hf)/Sm to have caused the arc-like signature of the SB rocks.

In the Buchanan Lake sample series, Rb/Ba is roughly correlated with the Pb/(Ce+Pr) and (Th+U)/(Nb+Ta) ratios, indicating a possible UCC involvement in about half of these samples with the positive Pb-anomalies (Fig S8). The same correlations, however, are not present in the correspondingly heterogeneous Lightfoot River group. In the remaining groups, arc-like patterns with high Pb/(Ce+Pr) and (Th+U)/(Nb+Ta) ratios are associated with high Rb/Ba ratios in the samples from Artharber Creek and the Strand Fjord Formation and low ratios in Rollrock River and Blue Mountain samples. These features are difficult to explain and could possibly be related to element mobility during secondary alteration. The lack of positive correlation between the Ba/Rb and Sr/(Pr+Nd) ratios in the relatively evolved SB basaltic rocks also preclude Ba-extraction during plagioclase fractionation (e.g. Blundy and Wood, 1991).

The limited Sr-Nd-isotopic data on rocks from the LP- and HP-series of the Hassel formation and from the Isachsen and Strand Fjord Formations published by Estrada (2014) can be used in a further attempt to identify SB rocks from mantle sources with or without arc signatures and with or without UCC assimilation effects (Fig. S11). The Hassel LP-series has a fertile mantle composition with time-corrected initial ε_{Nd} and $^{87}Sr/^{86}Sr$ of about +5 and 0.704, respectively. The negative Pb-anomalies (low Pb/(Ce+Pr) ratio) and low (Th+U)/(Nb+Ta) ratios in these basalts may indicate a HIMU-

source with a recycled oceanic crust component. The other SB rocks analyzed are displaced towards lower ε_{Nd} and higher $^{87}Sr/^{86}Sr$ with the Isachsen Fm., the Strand Fjord Fm. and the Hassel HP-group having values of about +4 and 0.7055, +2 and 0.707 and -1.4 and 0.707, respectively. This is well within the common range of island arc basalts (e.g. Fig. 16.12 in Winter, 2010) but could also be due to minor UCC assimilation as suggested by Estrada (2014). It is interesting to note that the change from the LP- to the HP-series of the Hassel Fm. is characterized by enrichment of Rb, Ba, Th, U, Pb, and the light intermediate REE, especially Eu, depletion of Nb, Ta, Zr and Hf and almost unaffected Sr (Fig. S7). Such a change is not expected from average UCC contamination but could possibly result from arc mantle contribution in the melting zone. The origin of the conspicuously elevated Eu content is unknown.

Supplementary Figures:

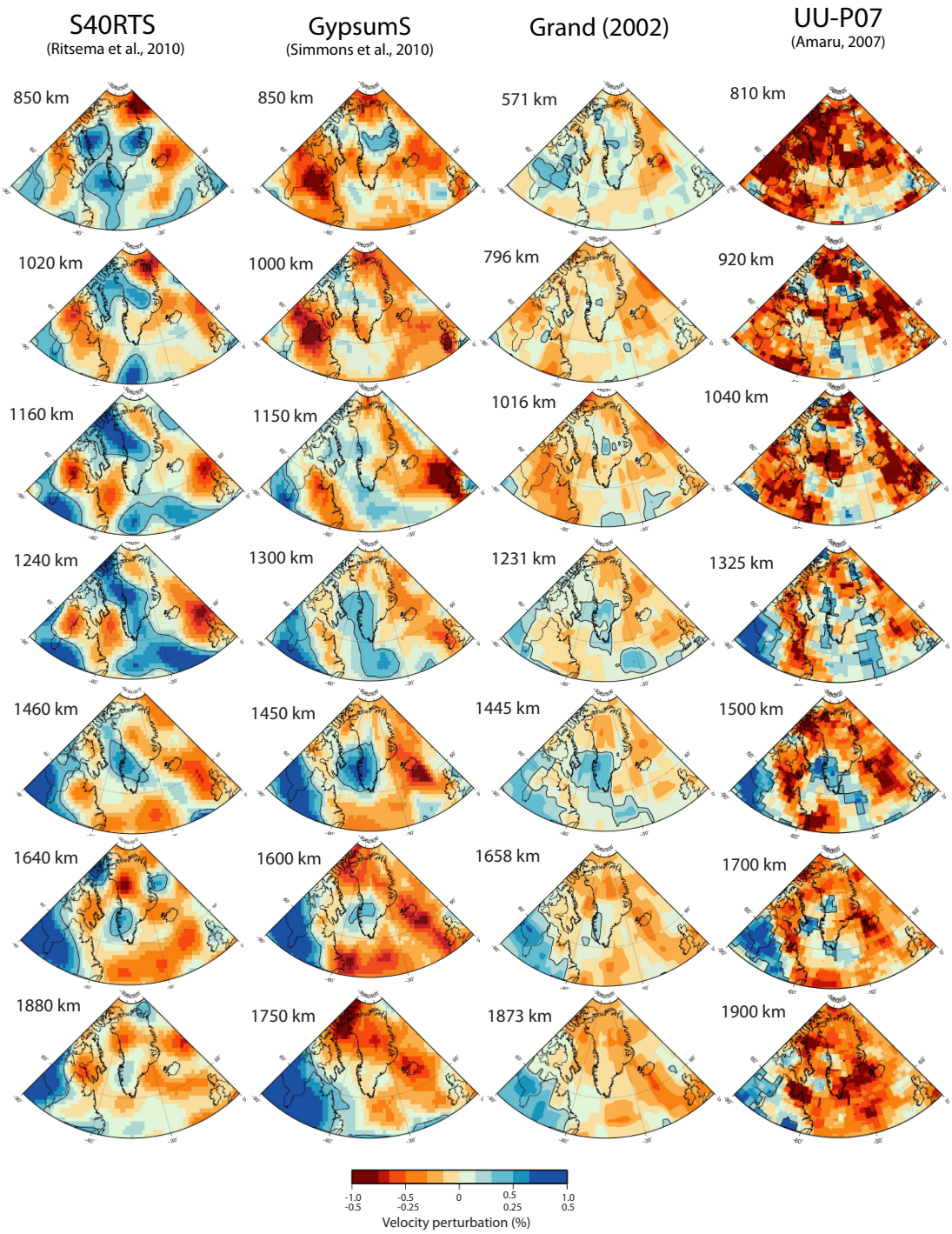

Figure S1. Complementary to Fig. 2; additional horizontal depth slices through seismic tomography models including Grand (2002).

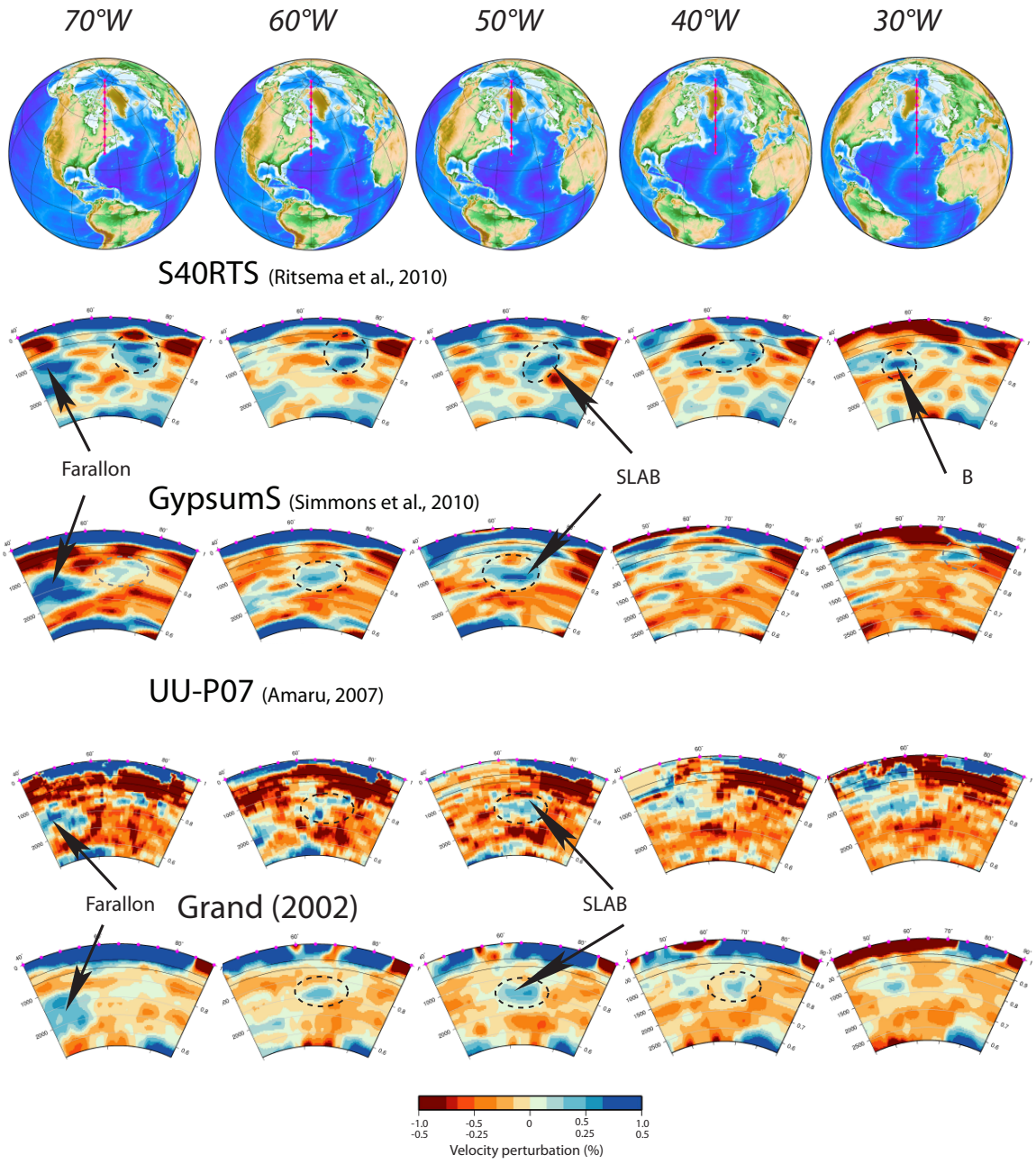

Figure S2. Complementary to Fig. 2; additional vertical slices through alternative seismic tomography models including Grand (2002), along varying line of latitude. Black circle identifies the location of the Greenland "SLAB" as discussed in text, as well as the "Farallon" slab and a possible extended anomaly "B". Note the location of the "SLAB" broadly between approximately 1000-1600 km depth, 70-40°W and 60-70°N. Across all of the tomography models the Greenland anomaly around ~1200-1300 km depth appears

to extend from under Baffin Bay to the SE towards Ireland. This is possibly an anomaly associated with the Greenland anomaly but its restricted depth range (between ~1200-1300 km) and far easterly location from any known palaeo-subduction zone or ocean basin (see Fig. 1B, S5 panel B) requires further analysis.

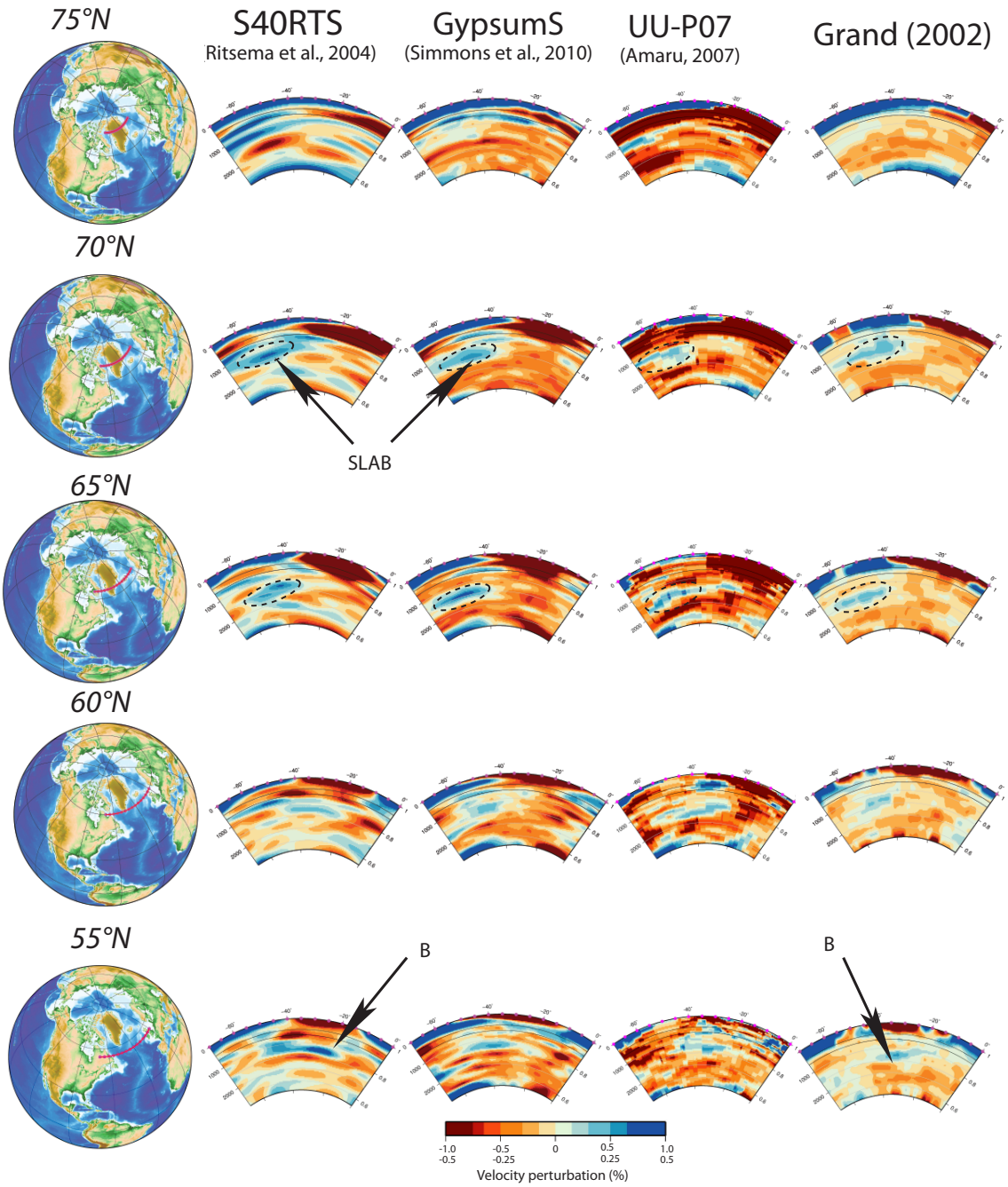

Figure S3. As in S2 but along varying line of longitude.

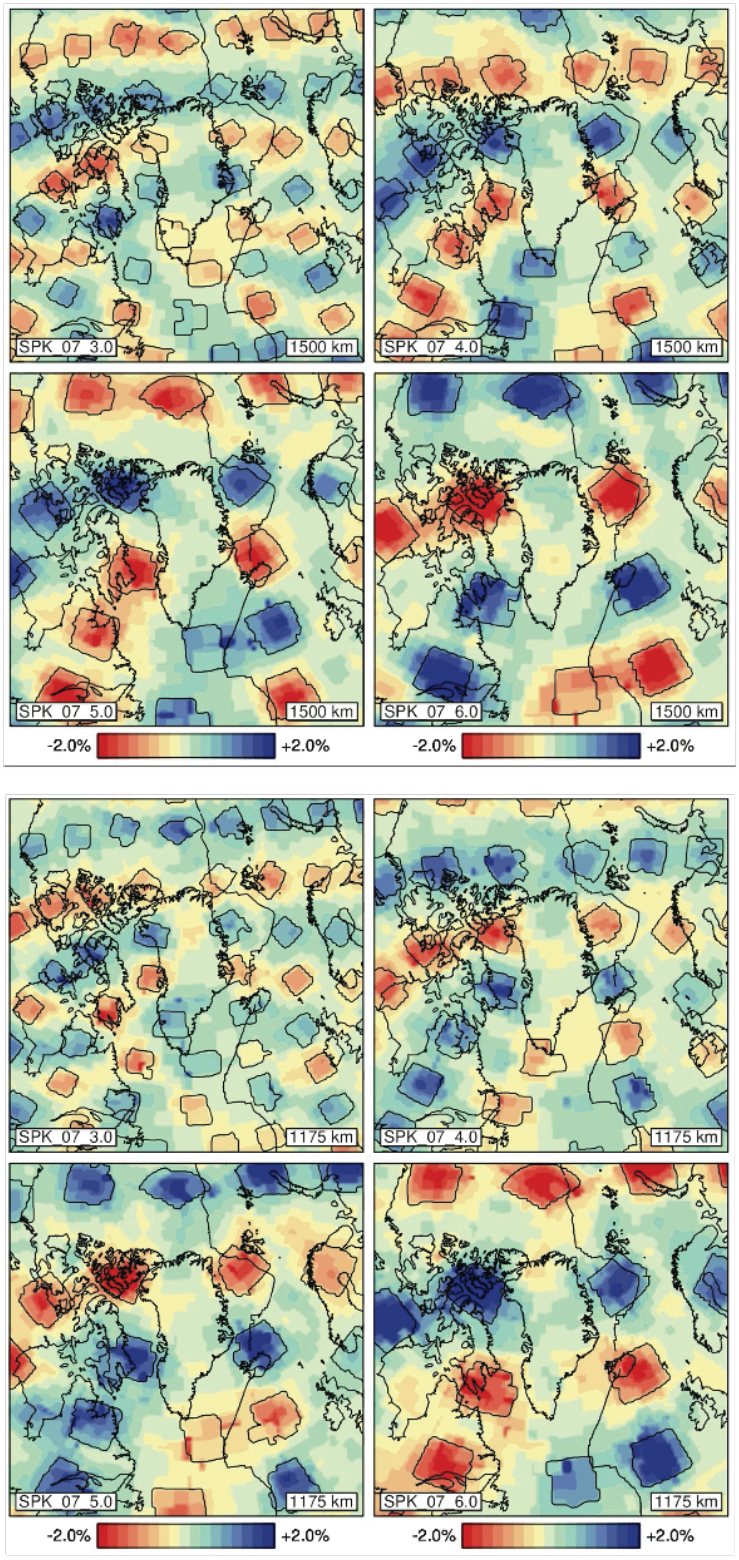

Figure S4. Checkboard test for the UU-P07 seismic tomography model (Amaru, 2007) at two different depths (1175 km and 1500 km) for 3.0, 4.0, 5.0 and 0.6 degrees.

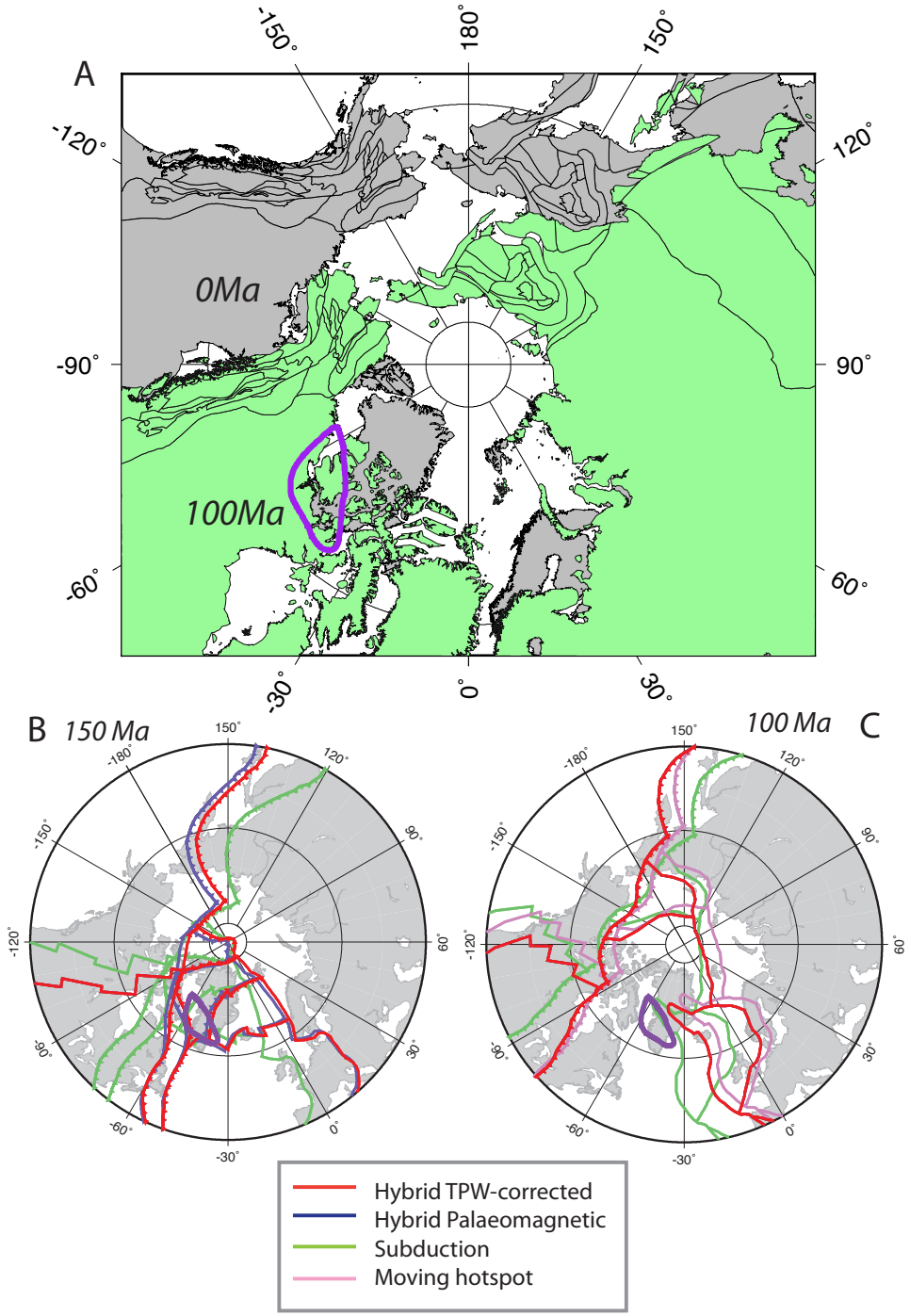

Figure S5. Panel A: comparison of present-day continental locations (grey) and those at 100 Ma (green). Thick purple contour of Greenland slab at 1460 km depth from S40RTS illustrating that the slab is not near the continental margin of NAM at 100 Ma, thus is likely a feature subducted earlier (as might be argued for faster sinking rates).

Panels B and C: comparison of four alternative absolute reference frames at 150 Ma and 100 Ma, respectively. Red, hybrid moving hotspot (O'Neill et al., 2005) and TPW model;

blue a palaeomagnetic model (Torsvik et al., 2008); green, a subduction reference frame (van der Meer et al., 2010), which is similar to the TPW model but with a longitudinal correction applied and; pink, a new moving hotspot model which only goes back as far as 124 Ma (Doubrovine et al., 2012). The choice of absolute reference frame could potentially account for an offset in subduction location and slab location (assuming vertical sinking). However, at the proposed time of subduction (after 160Ma) there is relatively minimal difference between three chosen reference frames at this Arctic location. Furthermore, the base reference frame used here (hybrid True-Polar Wander corrected reference frame [Steinberger and Torsvik, 2008] for times older than 100 Ma and a moving hotspot reference frame for 0-100 Ma [O'Neill et al., 2005]) predicts subduction boundaries the furthest east at this location compared to alternative reference frame i.e. the slab is not likely accounted for by a subduction zone further east than shown discussed here.

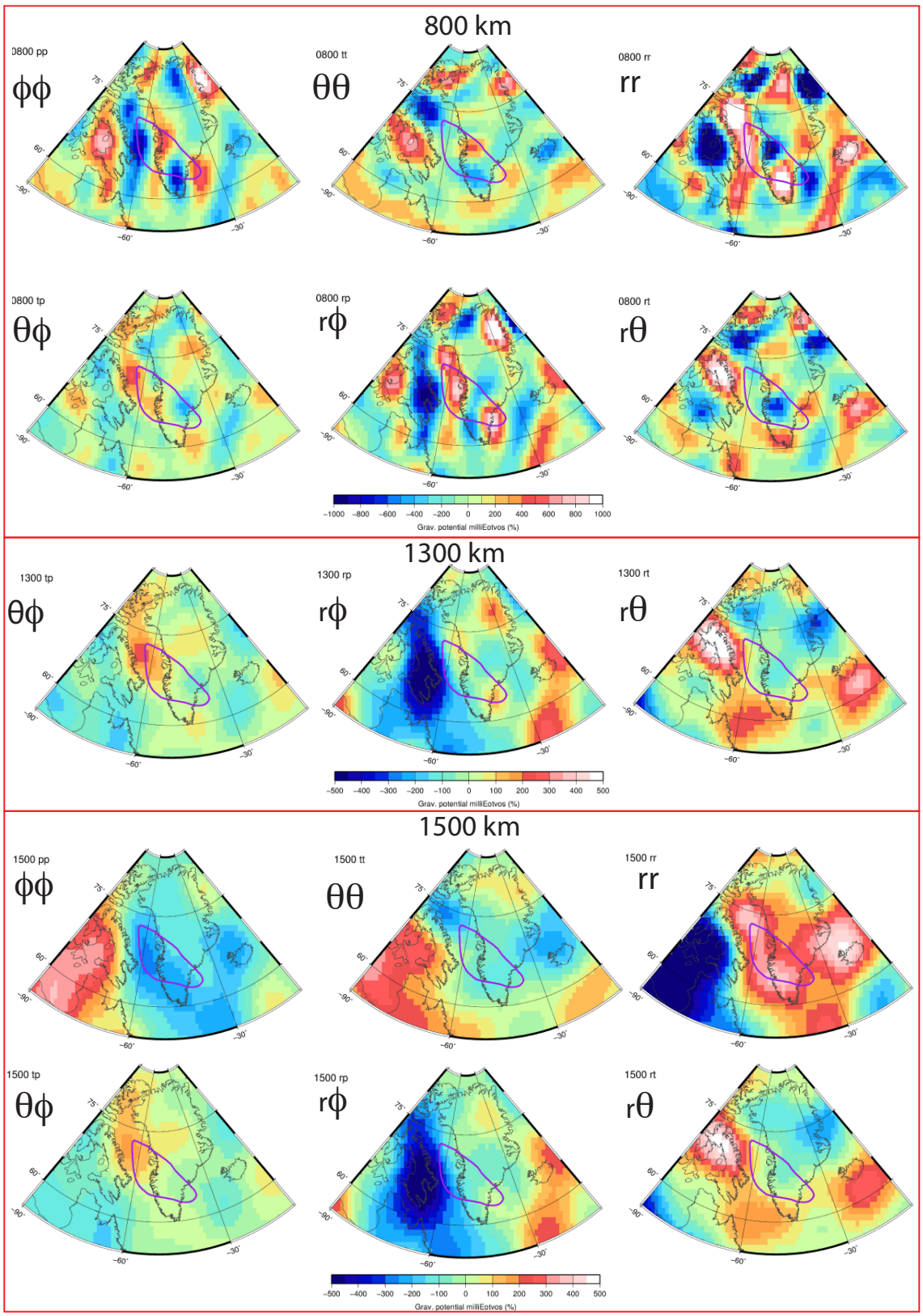

Figure S6. Complementary to Fig. 4. Gravity gradients from 800, 1300 and 1500 km wavelengths overlain with present-day coastlines (thin grey) and slab contours (0.3%)

derived from S40RTS at 1460 km. Gravity directions ϕϕ, θθ, and rr underline mantle mass features which show N-S, E-W and radial variations, respectively. Direction rθ similar to direction θθ but with radial component (less directional sensitivity), rϕ is similar to ϕϕ but with radial component (less directional sensitivity) and θϕ is a N-S component changing in an E-W direction.

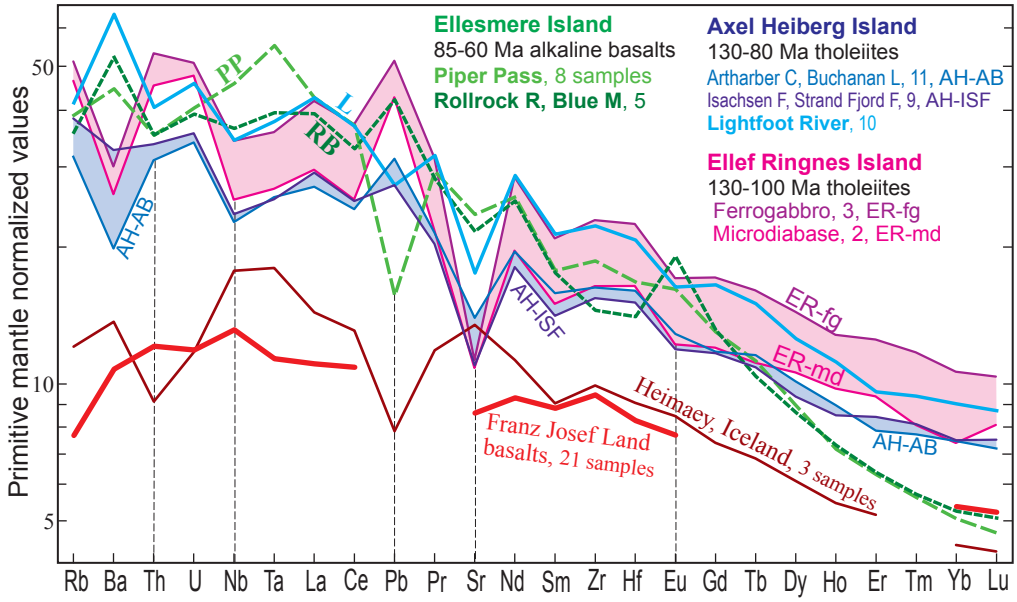

Figure S7. Trace element concentrations normalized to primitive mantle (Sun and McDonough, 1989) for HALIP basaltic rocks from Ellef Ringnes (Evenchick et al. 2015), Ellesmere and Axel Heiberg Islands (Jowitt et al. 2014; Estrada 2014) and Franz Josef Land (FJL, Ntaflos and Richter, 2003). Samples from the Vestmanaeyjar system (Heimaey, Iceland) with a strong recycled oceanic lithosphere signature (ROC/HIMU) are included for comparison (Peate et al. 2009). After removal of the evolved and fractionated samples with <4.5 wt% MgO, the rocks from the same formations and areas were grouped and averaged (sample number shown). Trace element patterns for the individual samples are shown in Supplementary Figs. S8 and S9. Legend abbreviations: R, River; M, Mountain; C, Creek; L, Lake; F, Formation.

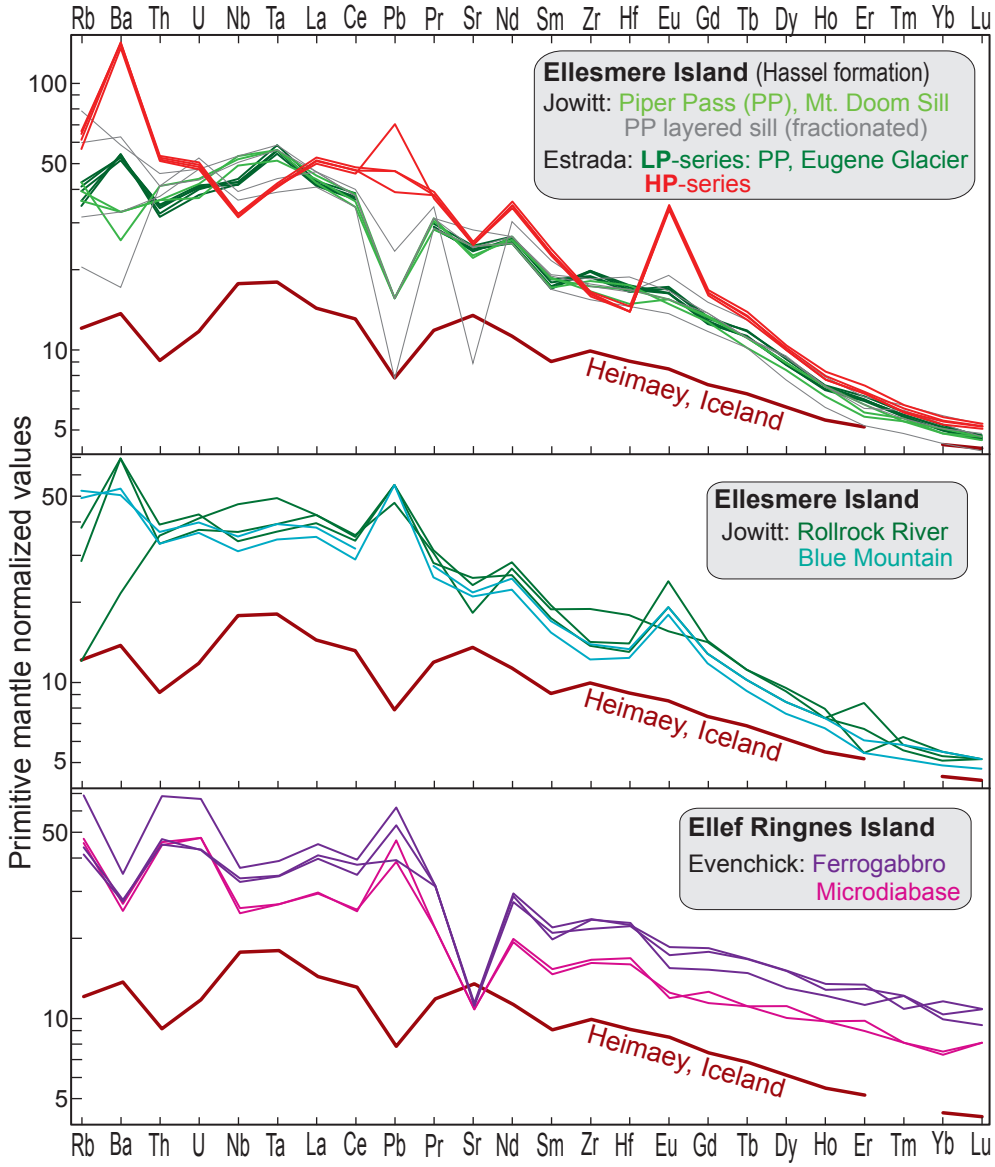

Figure S8. Trace element concentrations normalized to primitive mantle (Sun and McDonough, 1989) for HALIP samples from Ellesmere Island (Jowitt et al. 2014; Estrada 2014) and Ellef Ringnes Island (Evenchick et al. 2015). Heimaey (Vestmanaeyjar, Iceland, Peate et al., 2010) is included as a reference pattern in all the panels. ***Top panel***: Hassel formation, including the low-phophorous (LP-series) from the Piper Pass (PP) and Eugene Glacier areas. The PP layered sill samples are strongly fractionated and not included in the main Fig. 5 average. The samples in Figs. S7-S9 are filtered for samples with < 4.5wt% MgO. The exception is the high-P (HP) rocks of the Hassel formation

(3.6-3.8 wt% MgO), which are included here, because they are also plotted in the Nd-Sr-isotope Fig. S5. The HP rocks are not included in Figs. 5 and S7.

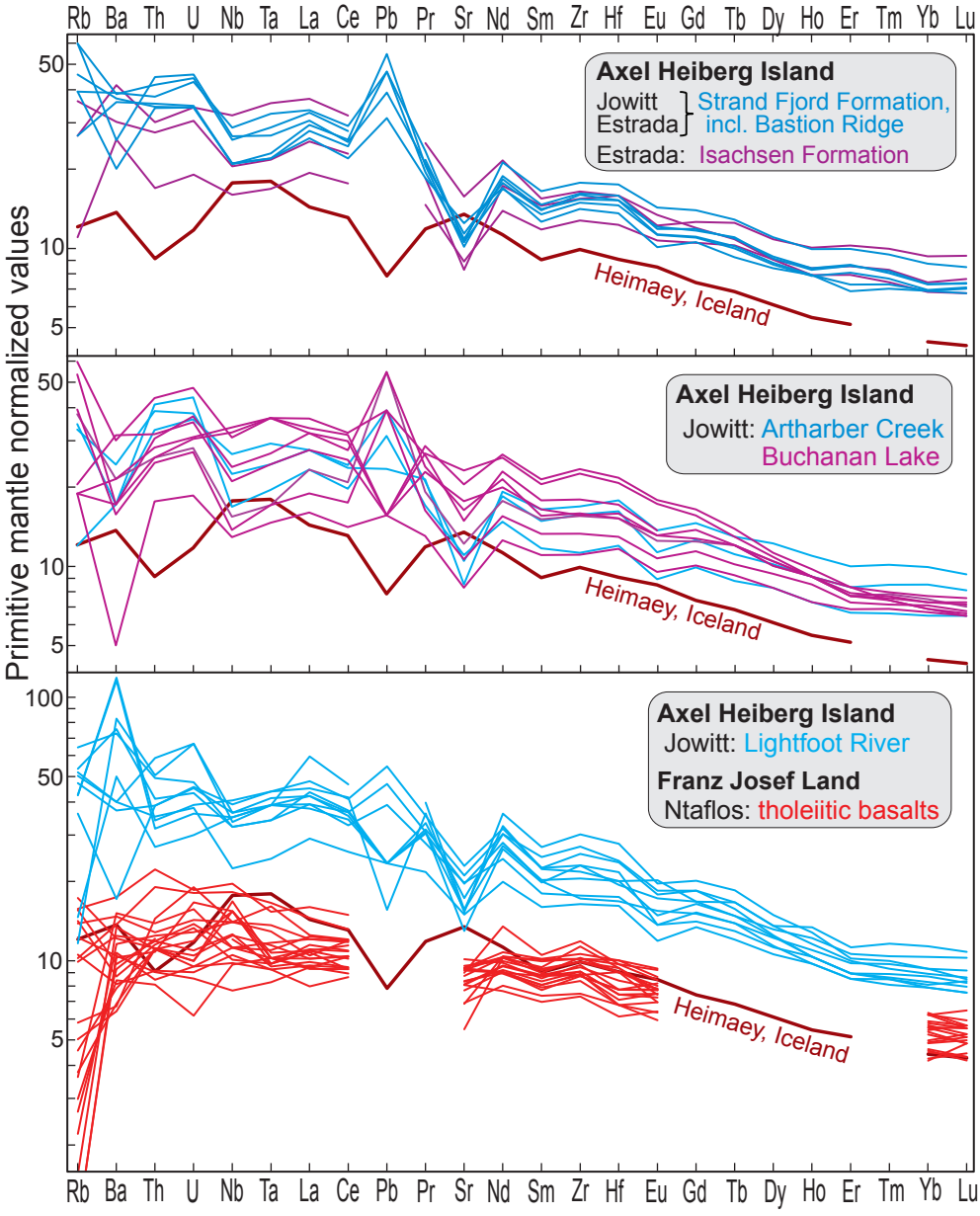

Figure S9. Trace element concentrations normalized to primitive mantle (Sun and McDonough, 1989) for HALIP samples from Axel Heiberg Island (Jowitt et al. 2014; Estrada 2014) and Franz Josef Land (Ntaflos and Richter 2003).

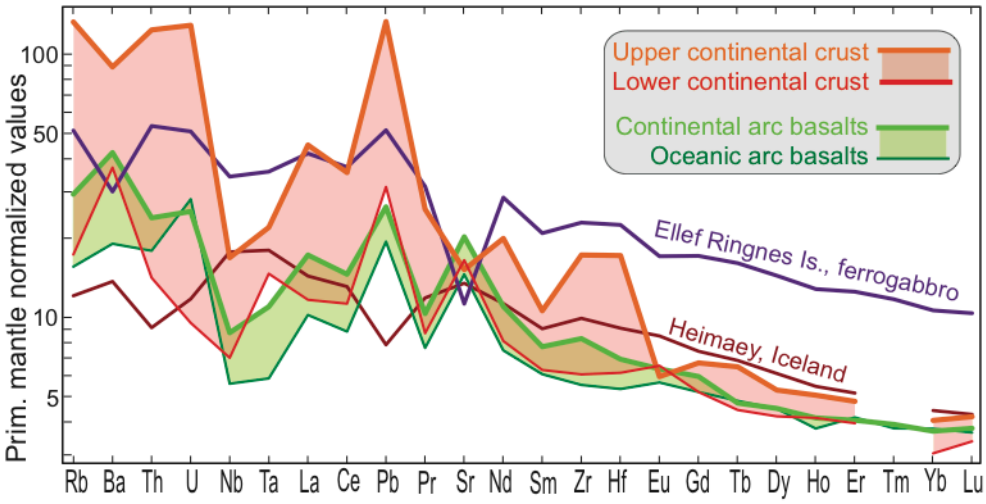

Figure S10. Normalized trace element concentration patterns of upper and lower continental crust (averages from Rudnick and Gao, 2003) and continental and oceanic arc basalts (averages from Keleman et al. 2003) compared to the Heimaey (Iceland) reference and the average of the three ferrogabbros from Ellef Ringnes Island (Peate et al. 2010; Evenchick et al. 2015; Figs. 5, S7 and S8).

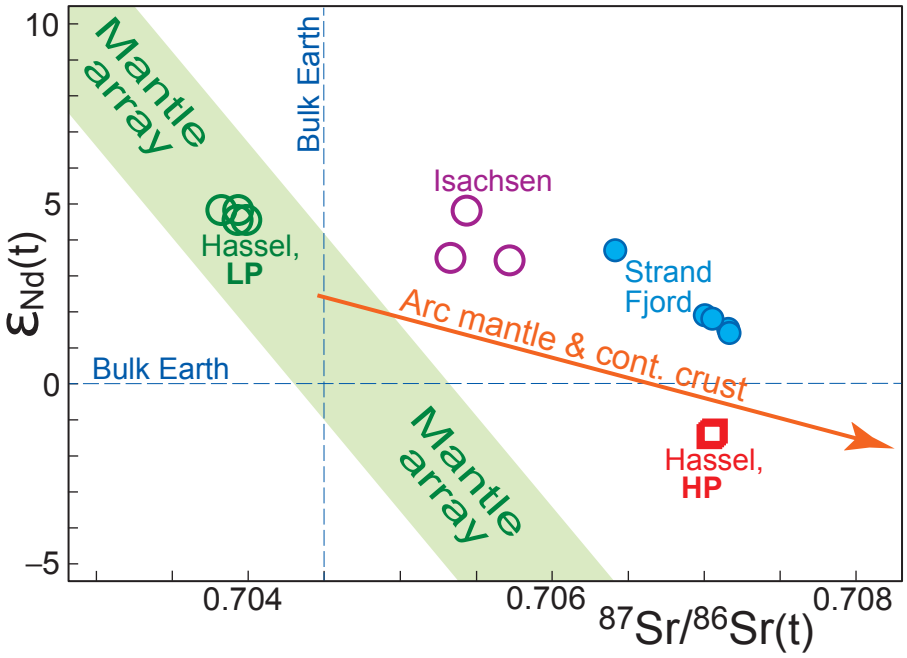

Figure S11. Initial Sr-Nd-isotope compositions (corrected to the rock ages) of samples from the Hassel, Isachsen and Strand Fjord formations from Estrada (2014). LP and HP: Low- and High-phosphorus rock series of the Hassel formation.

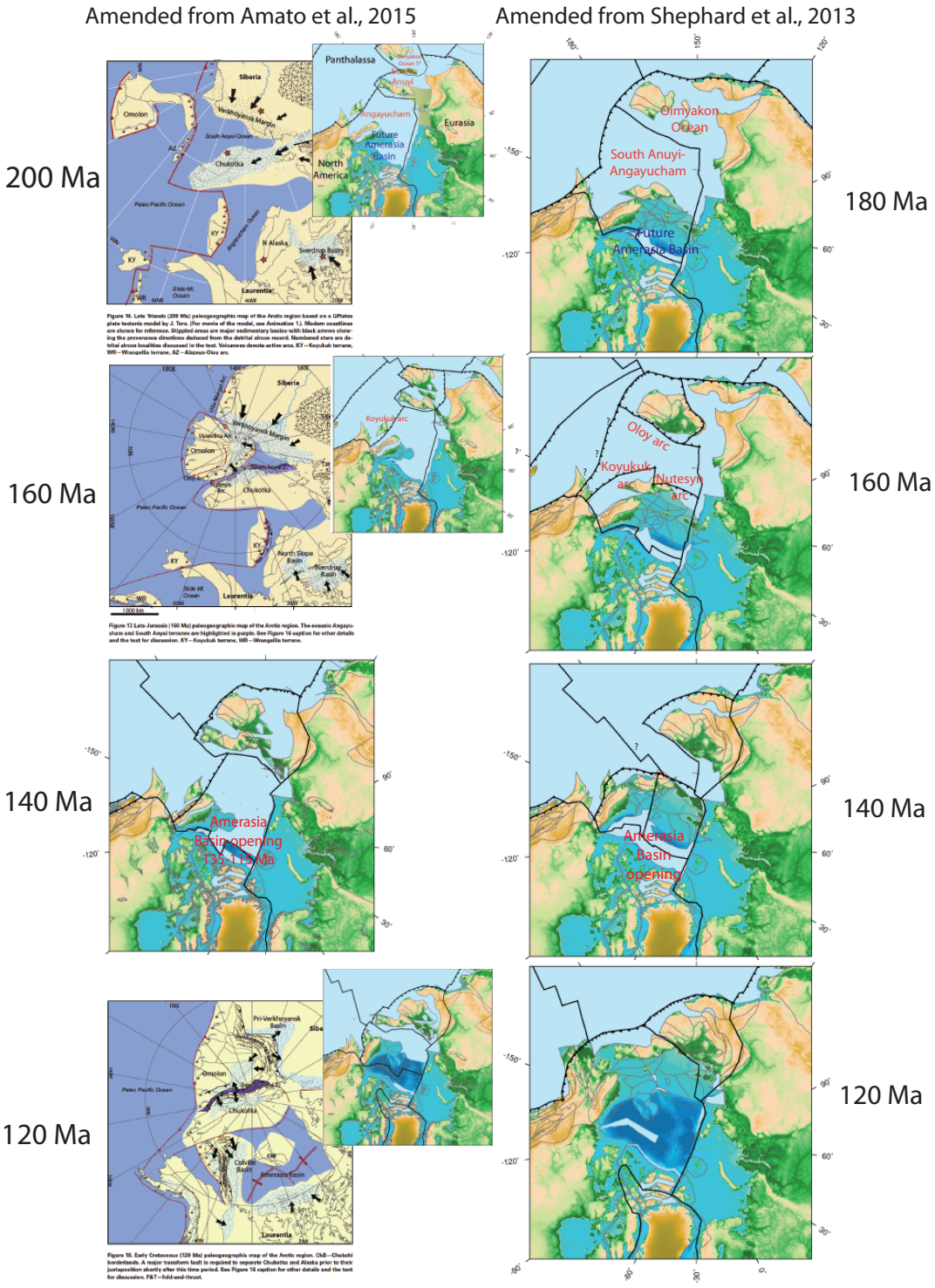

Figure S12. Schematic comparison of two alternative scenarios for the South Anuyi-Angayucham Ocean geometry, location and subduction history. Rightmost panels show reconstruction from Shephard et al. (2013) with a singular South Anuyi-Angayucham

Ocean due to a connected Chukotka-NSA. This model is based on several reconstructions including but not limited to Plafker and Berg (1994), Nokleberg et al. (2000), Grantz et al. (2011), Sokolov et al. (2002), Lawver et al. (2002). Continental terranes are exported having been cookie-cut to the (present-day) ETOPO2 raster. Plate boundaries in black. Leftmost panels, figures from Amato et al. (2015) depicting separate terranes of Chukotka and North Slope of Alaska and two oceans. Both reconstructions include subduction along the south-dipping Koyukuk arc as well as subduction associated with the opening of the Amerasia Basin. Inset of the left panels is an attempt to convert their reconstructions into the equivalent global model with connected plate boundaries as shown on the right (same projection, fixed North America reference frame). Note, that this is only a guideline and not a precise attempt to recreate the Amato et al. (2015) illustrations. We refer the reader to the manuscript and supplementary information. In particular, difficulty lies in generating consistent plate boundaries and velocities as well as a consideration of the age of oceanic lithosphere and the complete restoration of continental versus oceanic terranes in the intervening areas. Nonetheless, the timing of regional subduction in the high Arctic from at least 160-120 Ma, with the latest stage being consistent with Amerasia Basin opening, does not change the our interpretation of the Greenland slab affinity.

Supplementary References

Amato, J. M., Toro, J., Akinin, V. V., Hampton, B. A., Salnikov, A. S., and Tuchkova, M. I., in press, Tectonic evolution of the Mesozoic South Anyui suture zone, eastern Russia: A critical component of paleogeographic reconstructions of the Arctic region: *Geosphere* 11(5) 33pp. doi:10.1130/GES01165.1

Amaru, M. L. (2007), Global travel time tomography with 3-D reference models: Geologica Ultraiectina, v. 274, p. 174.

Blundy, J. D. and B. J. Wood (1991), Crystal-chemical controls on the partitioning of Sr and Ba between plagioclase feldspar, silicate melts, and hydrothermal solutions. Geochimica et Cosmochimica Acta, 55, 193-209.

Doubrovine, P. V., B. Steinberger, and T.H. Torsvik (2012), Absolute plate motions in a reference frame defined by moving hot spots in the Pacific, Atlantic, and Indian oceans: Journal of Geophysical Research: Solid Earth, v. 117, no. B9, p. B09101.

Dziewonski, A. M., and D.L. Anderson (1981), Preliminary reference Earth model: Physics of the Earth and Planetary Interiors, v. 25, no. 4, p. 297-356.

Estrada, S. (2014), Geochemical and Sr–Nd isotope variations within Cretaceous continental flood-basalt suites of the Canadian High Arctic, with a focus on the Hassel Formation basalts of northeast Ellesmere Island. *Int. J. Earth Sci.*, 10.1007/s00531-014-1066-x

Evenchick, C. A., W.J. Davis, J. H Bedard, N. Hayward and R.M. Friedman (2015), Evidence for protracted High Arctic large igneous province magmatism in the central Sverdrup Basin from stratigraphy, geochronology, and paleodepths of saucer-shaped sills. Geological Society of America, Bulletin doi: 10.1130/B31190.1

Grand, S. P. (2002), Mantle shear–wave tomography and the fate of subducted slabs, v. 1800, 2475-2491 p.:

Grantz, A., Hart, P.E., Childers, V.A., 2011b. Geology and tectonic development of the Amerasia and Canada Basins, Arctic Ocean. In: Spencer, A.M., Embry, A.F., Gautier, D.L., Stoupakova, A.V., Sørenson, K. (Eds.), Arctic Petroleum Geology. Geological Society, London, Memoirs, vol. 35, pp. 771–799. http://dx.doi.org/10.1144/

M35.50 (Chapter 50).Hofmann, A. W. (1997), Mantle geochemistry: the message from oceanic volcanism, Nature, 385(6613), 219-229.

Jowitt, S. M., M.-C.Williamson and R.E. Ernst (2014), Geochemistry of the 130 to 80 Ma Canadian High Arctic Large Igneous Province (HALIP) Event and Implications for Ni-Cu-PGE Prospectivity: Economic Geology, v. 109, no. 2, p. 281-307.doi: 10.2113/econgeo.109.2.281

Keleman, P. B., K. Hanghøj, A. R. Greene (2003), 3.18 - One View of the Geochemistry of Subduction-related Magmatic Arcs, with an Emphasis on Primitive Andesite and Lower Crust, in *Treatise on Geochemistry*, edited by H. D. H. K. Turekian, pp. 593-659, Pergamon, Oxford.

Kennett, B. L. N., E. R. Engdahl and R. Buland (1995), Constraints on seismic velocities in the Earth from traveltimes: Geophysical Journal International, v. 122, no. 1, p. 108-124.

Lawver, L.A., Grantz, A., Gahagan, L.M., 2002. Plate kinematic evolution of the present Arctic region since the Ordovician. In: Miller, E.L., Grantz, A., Klemperer, S.L. (Eds.), Tectonic Evolution of the Bering Shelf–Chukchi Sea–Arctic Margin and Adjacent Land Masses. Special Papers, 360. Geological Society of America, Boulder, Colorado, pp. 333–358

Manning, C. E. (2004), The chemistry of subduction-zone fluids, Earth and Planetary Science Letters, 223(1–2), 1-16.

Nokleberg, W.J., Parfenov, L.M., Monger, J.W.H., Norton, I.O., Khanchuk, A.I., Stone, D.B., Scotese, C.R., Scholl, D.W., Fujita, K., 2000. Phanerozoic tectonic evolution of the Circum-North Pacific. Professional Paper 1626.U.S. Geological Survey (122 pp.).

Ntaflos, T., and W. Richter (2003), Geochemical constraints on the origin of the continental flood basalt magmatism in Franz Josef Land, Arctic Russia, *Eur. J. Mineral 15*(4), 649-663.

O'Neill, C., D. Müller and B. Steinberger (2003) Geodynamic implications of moving Indian Ocean hotspots: Earth and Planetary Science Letters, v. 215, no. 1–2, p. 151-168.

Panet, I., G. Pajot-Metivier, M. Greff-Lefftz, L. Metivier, M. Diament, and M. Mandea (2014), Mapping the mass distribution of Earth/'s mantle using satellite-derived gravity gradients, *Nature Geosci*, *7*(2), 131-135.

Peate, D. W., K. Breddam, J. A. Baker, M. D. Kurz, A. K. Barker, T. Prestvik, N. Grassineau, and A. C. Skovgaard (2010), Compositional Characteristics and Spatial Distribution of Enriched Icelandic Mantle Components, Journal of Petrology, 51(7), 1447-1475.

Plafker, G., Berg, H.C., 1994. Overview of the geology and tectonic evolution of Alaska. The Geology of North America Vol. G-I. Geological Society of America Special Paper, 442, pp. 121–131.

Poli, S., and Schmidt, M.W., 2002, Petrology of subducted slabs Annual Review of Earth and Planetary Sciences, v. 30, p. 207-235. doi: 10.1146/annurev.earth.30.091201.140550

Ritsema, J., A. Deuss, H. J. van Heijst, and J. H. Woodhouse (2011), S40RTS: a degree-40 shear-velocity model for the mantle from new Rayleigh wave dispersion, teleseismic traveltime and normal-mode splitting function measurements, *Geophysical Journal International*, *184*(3), 1223-1236.

Rudnick, R. L., and S. Gao (2003), 3.01 - Composition of the Continental Crust, in *Treatise on Geochemistry*, edited by H. D. H. K. Turekian, pp. 1-64, Pergamon, Oxford.

Simmons, N. A., A. M. Forte, L.Boschi and S. P. Grand (2010) GyPSuM: A joint tomographic model of mantle density and seismic wave speeds: Journal of Geophysical Research: Solid Earth, v. 115, no. B12, p. B12310.

Sokolov, S.D., Bondarenko, G.Y., Morozov, O.L., Shekhovtsov, V.A., Glotov, S.P., Ganelin, A.V., Kravchenko-Berezhnoy, I.R., 2002. South Anyui Suture, northeast Arctic Russia: facts and problems. In: Miller, E.L., Grantz, A., Klemperer, S.L. (Eds.), Tectonic Evolution of the Bering Shelf–Chukchi Sea–Arctic Margin and Adjacent Land Masses. Special Papers, 360. Geological Society of America, Boulder, Colorado, pp. 209–224.

Steinberger, B., and T. H. Torsvik (2008) Absolute plate motions and true polar wander in the absence of hotspot tracks: Nature, v. 452, no. 7187, p. 620-623.

Sun, S.-s., and W. F. McDonough (1989), Chemical and isotopic systematics of oceanic basalts: implications for mantle composition and processes, Geological Society, London, Special Publications, 42(1), 313-345.

Torsvik, T. H., M. A. Smethurst, K.Burke, and B. Steinberger (2008) Long term stability in deep mantle structure: Evidence from the ~ 300 Ma Skagerrak-Centered Large Igneous Province (the SCLIP): Earth and Planetary Science Letters, v. 267, no. 3–4, p. 444-452.

Trønnes, R. G., V. Debaille, M. Erambert, F. M. Stuart, and T. Waight (2013), Mixing and progressive melting of deep and shallow mantle sources in the NE Atlantic and Arctic, *Mineralogical Magazine*, *77*(5), 2357.

van der Meer, D. G., W. Spakman, D. J. J. van Hinsbergen, M. L. Amaru, and T.H. Torsvik (2010). Towards absolute plate motions constrained by lower-mantle slab remnants: Nature Geosci, v. 3, no. 1, p. 36-40.

Winter, J. D. (2010) Principles of Igneous and Metamorphic Petrology. 2nd. Ed. Prentice Hall, Pearson, 702 pp.

Woo, Y., K. Yang, Y. Kil, S.-H. Yun, and S. Arai (2014), Silica- and LREE-enriched spinel peridotite xenoliths from the Quaternary intraplate alkali basalt, Jeju Island, South Korea: Old subarc fragments?, Lithos, 208–209(0), 312-323.